Cell Reports

Article

Stability of ripple events during task engagement in human hippocampus

Graphical abstract

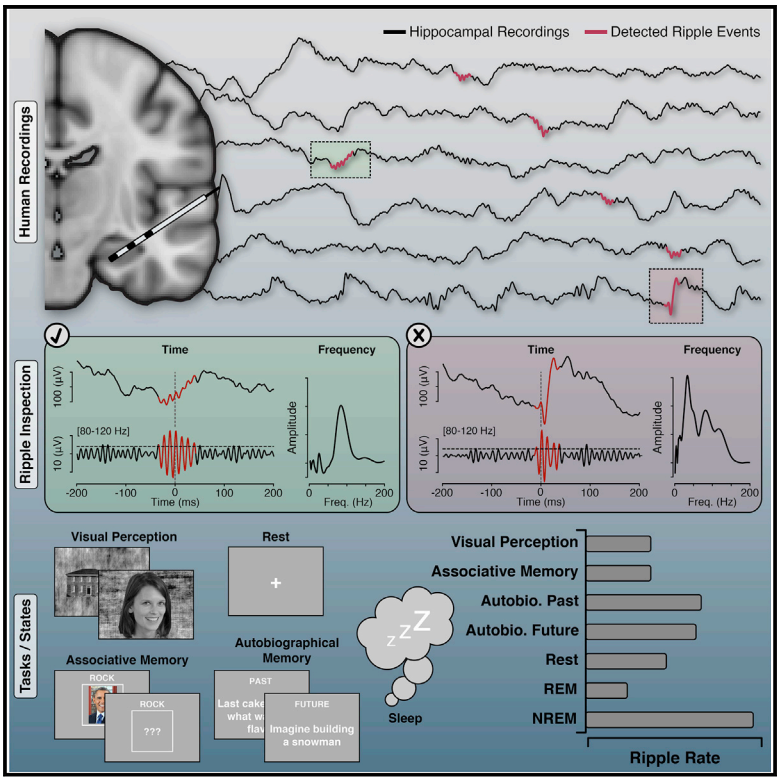

Highlights

- Hippocampal ripple detection is improved by time-frequency verification
- Ripples occur in human hippocampus during various awake cognitive states at a low rate
- Ripple rates are stable across perceptual and associative memory tasks
- Ripple rates are enhanced during complex autobiographical memory retrieval

Authors

Yvonne Y. Chen, Lyndsey Aponik-Gremillion, Eleonora Bartoli, Daniel Yoshor, Sameer A. Sheth, Brett L. Foster

Correspondence

brett.foster@pennmedicine.upenn.edu

In brief

Hippocampal ripples are high-frequency activity bursts proposed to support "offline" memory consolidation. Chen et al. identify that human hippocampal ripples occur with stable properties across tasks of visual perception and associative memory but are enhanced for autobiographical memory retrieval and non-REM sleep, supporting their "online" role in establishing and strengthening memory traces.

Chen et al., 2021, Cell Reports *35*, 109304
June 29, 2021
https://doi.org/10.1016/j.celrep.2021.109304

CellPress

Cell Reports

CellPress
OPEN ACCESS

Article

Stability of ripple events during task engagement in human hippocampus

Yvonne Y. Chen,[1,3] Lyndsey Aponik-Gremillion,[1,2] Eleonora Bartoli,[1] Daniel Yoshor,[3] Sameer A. Sheth,[1,2] and Brett L. Foster[1,2,3,4,*]

[1]Department of Neurosurgery, Baylor College of Medicine, 1 Baylor Plaza, Houston, TX 77030, USA
[2]Department of Neuroscience, Baylor College of Medicine, 1 Baylor Plaza, Houston, TX 77030, USA
[3]Department of Neurosurgery, Perelman School of Medicine, University of Pennsylvania, 3400 Spruce Street, Philadelphia, PA 19104, USA
[4]Lead contact
*Correspondence: brett.foster@pennmedicine.upenn.edu
https://doi.org/10.1016/j.celrep.2021.109304

SUMMARY

High-frequency activity bursts in the hippocampus, known as ripples, are thought to support memory consolidation during "offline" states, such as sleep. Recently, human hippocampal ripples have been observed during "online" episodic memory tasks. It remains unclear whether similar ripple activity occurs during other cognitive states, including different types of episodic memory. However, identifying genuine ripple events in the human hippocampus is challenging. To address these questions, spectro-temporal ripple identification was applied to human hippocampal recordings across a variety of cognitive tasks. Overall, ripple attributes were stable across tasks of visual perception and associative memory, with mean rates lower than offline states of rest and sleep. In contrast, while more complex visual attention tasks did not modulate ripple attributes, rates were enhanced for more complex autobiographical memory conditions. Therefore, hippocampal ripples reliably occur across cognitive states but are specifically enhanced during offline states and complex memory processes, consistent with a role in consolidation.

INTRODUCTION

Long-term memory formation is thought to be supported by consolidation processes occurring during "offline" states, the most prominent being sleep (Klinzing et al., 2019). During sleep, a host of electrographic signatures are reliably observed in the hippocampus and neocortex, which are thought to underlie systems memory consolidation (Diekelmann and Born, 2010; Joo and Frank, 2018; Klinzing et al., 2019). Specifically, during non-rapid eye movement (NREM) sleep periods, high-frequency oscillations (~80–120 Hz in humans), known as ripples or sharp-wave ripples, are observed in the hippocampus (Bragin et al., 1999; Buzsáki, 2015; Helfrich et al., 2019; Jiang et al., 2019; Staresina et al., 2015). Furthermore, hippocampal ripples display a temporal coordination with other canonical NREM sleep signatures, including spindles (~12–16 Hz) and slow oscillations (<1 Hz) (Sirota et al., 2003; Staresina et al., 2015). As part of this orchestrated dynamic, hippocampal ripple events are thought to support interactions with the neocortex via a two-stage model for systems consolidation (Klinzing et al., 2019). Under this view, newly encountered information is initially encoded by the hippocampus, but progressively becomes consolidated in the neocortex (Chen and Wilson, 2017; Diekelmann and Born, 2010; Dudai et al., 2015).

While these consolidation processes are most pronounced during offline states, when cognitive engagement is thought to be reduced, recent findings build on prior work suggesting that similar electrographic signatures, particularly ripples, can be observed during awake states (Axmacher et al., 2008). Most recently, it has been reported that ripple events occur in the human hippocampus or medial temporal lobe (MTL) cortex during the performance of episodic memory tasks (Norman et al., 2019; Vaz et al., 2019). Interestingly, ripples were observed at rates equal to or greater than those typically observed during NREM sleep (Jiang et al., 2020; Ngo et al., 2020). Furthermore, hippocampal ripple events were associated with neocortical reinstatement activities and successful memory retrieval (Norman et al., 2019; Vaz et al., 2019). These findings suggest that hippocampal ripples may occur during active memory behavior, supporting hippocampal-neocortical interactions, similar to those observed during sleep (Joo and Frank, 2018).

In light of these findings, it is important to ascertain the specificity of online ripple events for memory behaviors that are typically associated with the hippocampus and other MTL regions. At present, there is limited evidence regarding how the occurrence of hippocampal ripples and their attributes differ across cognitive task states, including those not typically associated with episodic memory (Buzsáki, 2015). Ripple attributes, including rate, duration, and frequency, likely modulate the mechanistic impact of these events. Recently, Norman et al. (2019) reported that across different stages of a memory recall paradigm, ripple events were similar in amplitude and frequency, but differed slightly in rate, suggesting a general stability of attributes across online task states.

To sensitively assess ripple activity in the human hippocampus, direct invasive recordings are optimal. However, such recordings only typically occur within the context of monitoring being performed for the neurosurgical treatment of refractory epilepsy. This clinical context produces several confounds for the study of ripple activity that require attention, as hippocampal inter-ictal spikes associated with epileptogenic tissue produce transient amplitude increases over a broad frequency range, including the ripple band (Jiang et al., 2020). Therefore, careful consideration of these artifacts and their spectral signatures is required to confidently identify genuine hippocampal ripples and in turn their attributes across cognitive tasks.

In the present study, we examined hippocampal ripple attributes across cognitive tasks in 18 subjects undergoing invasive monitoring for epilepsy surgery. We report a striking stability of ripple attributes (rate, duration, amplitude, and frequency) across perceptual and associative memory tasks, while offline resting and sleep conditions showed an elevation in ripple rate. We observed no meaningful difference of these attributes based on anatomical factors within the hippocampus. Furthermore, we find that these attributes were stable throughout the time of day and proximity to electrode implantation. In general, we report that hippocampal ripples occur at significantly lower rates than have been previously reported for cognitive tasks. However, when considering the impact of more complex cognitive tasks, both perceptual and mnemonic, we find specific event-related increases in ripple rates for autobiographical memory conditions (past and future). We discuss these results within the broader context of how task-related ripple events may serve to establish hippocampal-neocortical dynamics that are later elevated during complex event retrieval and sleep to support memory consolidation.

RESULTS

Detected ripple events

Direct hippocampal recordings were performed in 18 subjects undergoing invasive monitoring for the surgical treatment of refractory epilepsy (see STAR Methods). Across subjects, a total of 139 electrodes were anatomically localized to the hippocampi. During recordings, subjects performed four tasks focused on visual object perception (perception), episodic memory encoding and retrieval (memory), eyes open/closed rest (resting), and an attention-episodic memory switch task (switch; additional supporting tasks described below). Using threshold-based ripple detection across these tasks, we identified a total of 13,520 ripple events, with 77.4% of these detected ripples subsequently being classified as genuine (10,465/13,520; see Figure 1 for examples of real and artifactual ripple events). In addition, after applying an electrode-rejection criterion, 82 electrodes were kept for our main analysis, resulting in a total of 7,831 ripples (mean ripple keep rate per electrode = 86.27%). See STAR Methods for ripple detection and rejection details.

To validate and benchmark ripple detection/rejection methods, we performed signal-based and location-based controls. First, to serve as the signal-based control, we created surrogate intracranial electroencephalogram (iEEG) data from an example hippocampal recording (subject S10, electrode 4; see Figure 1) using an iterative amplitude adjusted Fourier transform (iAAFT) approach (Lancaster et al., 2018). It is important to note that the generated surrogate data statistically matched the amplitude distribution and power spectrum of the original signal, while its temporal sequence was scrambled. Therefore, original "real" ripples would not be preserved in the hippocampal surrogate data (see STAR Methods for surrogate data generation details). After applying the same ripple detection/rejection method, we identified 3 ripple events from the hippocampal surrogate data (ripple rate = 0.007 Hz). Compared to the original hippocampal recording (ripple rate = 0.024 Hz), the ripple rate was drastically reduced (see Figures 1F and S1). Second, to serve as a location-based control, we performed ripple detection/rejection for a non-hippocampal cortical electrode (S10, same recording session as the examples shown in Figure 1; see Figure S1 for electrode anatomical location). After applying ripple detection/rejection, we identified 14 ripple events from the cortical data (ripple rate = 0.034 Hz). Interestingly, the cortical ripple rate was slightly elevated compared to the hippocampal electrode. As above, we generated the cortical surrogate data and applied ripple detection/rejection. We identified 13 ripple events from the cortical surrogate data (ripple rate = 0.031 Hz). Therefore, while ripple rates were overall lower in the hippocampus, the difference with the surrogate data was much greater than that observed in the cortex (suggesting a higher false detection rate in cortex).

Ripple attributes across different cognitive tasks

After applying time and frequency domain metrics for hippocampal ripple identification, we observed clear ripple events in all subjects and across all tasks. We sought to quantify ripple attributes across our three main tasks (perception, memory, and resting; Figure 2). As shown in Figure 2, hippocampal ripples were readily detected across all three tasks, displaying highly similar electrographic signatures (Figures 2E–2G). Given these similarities, we also quantified several other ripple attributes for comparison across tasks, which included: (1) rate (Hz, number of ripples per second), (2) duration (ms, time period ripple is above amplitude threshold), (3) amplitude (μV, max ripple amplitude), and (4) peak frequency (Hz, frequency with max amplitude within ripple band). Qualitatively, ripple attributes did not display any large differences across tasks. However, group linear mixed-effects analysis of ripple attributes, with tasks as a fixed effect and subject/electrode as random effects, revealed a significant main effect of task for rate, duration, and amplitude, but not for peak frequency (Satterthwaite approximations used for significance of model coefficients). Specifically, using pairwise Tukey's range test, with p values adjusted for comparing a family of 3 estimates, ripple rates were higher for resting than the other 2 tasks (resting-memory: $t(112) = 3.354$, $p = 0.0031$ and resting-perception: $t(112) = 2.522$, $p = 0.0348$); ripple duration was longer in resting than the other 2 tasks (resting-memory: $t(119) = 4.942$, $p < 0.0001$ and resting-perception: $t(119) = 4.659$, $p < 0.001$); and ripple amplitude was greater in resting than the other 2 tasks (resting-memory: $t(109) = 3.406$, $p = 0.0026$ and resting-perception: $t(109) = 2.192$, $p = 0.001$). Moreover, there was no significant difference between memory and perception tasks

CellPress
OPEN ACCESS

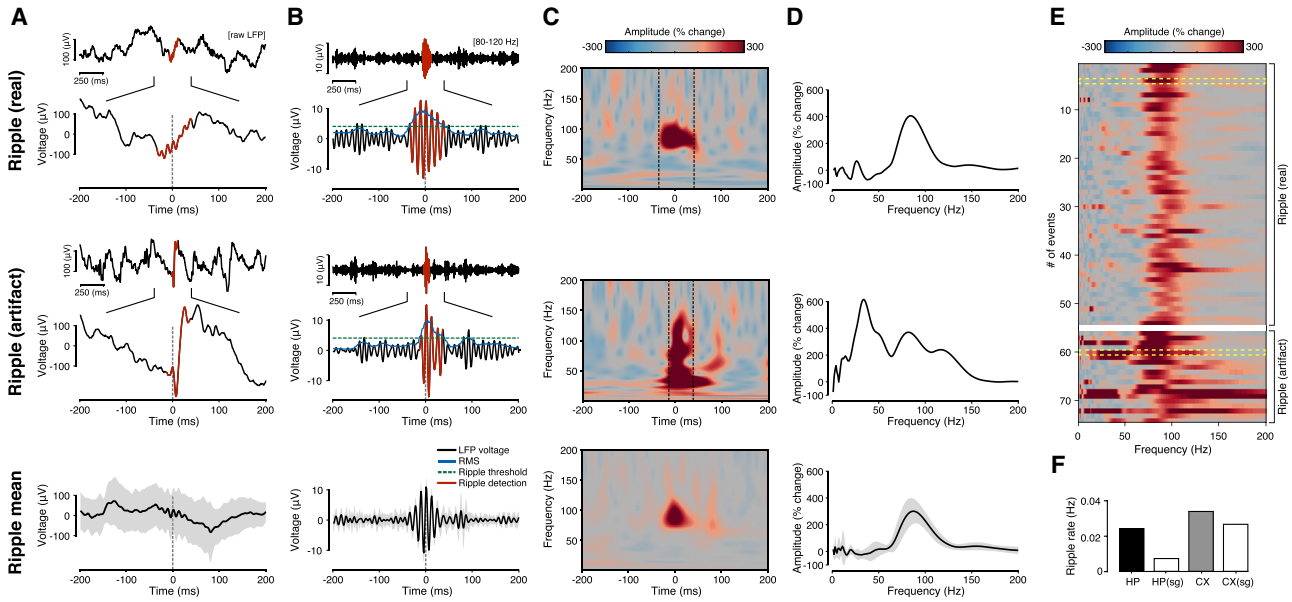

Figure 1. Ripple detection and artifact rejection

(A) Example raw voltage traces showing detected ripples that are subsequently identified as real (top) or artifactual (center), along with the mean ripple-triggered raw voltage trace after artifact rejection (bottom; here and below, error shading reflects SD; data from S10, electrode 4, perception task run 1; see Figure S1 for electrode location). Here and below, time zero aligns to the maximal ripple amplitude, with detected ripple events shown in red.

(B) Ripple-band (80–120 Hz) voltage traces for example real, artifactual, and mean ripples (same data as A). Green dashed line reflects the ripple detection threshold for this electrode. Blue line reflects the ripple-band RMS envelope.

(C) Spectrograms are shown for the example real, artifactual, and mean ripples; color maps reflect percentage change in amplitude relative to the total signal mean. Black dashed lines denote the onset and offset of detected ripples. Real ripple events display a high-frequency narrow band time-frequency representation, while the artifactual ripple displays a much more broadband frequency representation due to the sharp voltage transient shown in (A).

(D) Normalized amplitude spectra (percentage change) for the example real, artifactual, and mean ripples averaged over the detected ripple onset/offset window. While the real ripple displays a predominant spectral peak in the ripple-band range, the artifactual ripple shows multiple spectral peaks outside the ripple band. To isolate genuine ripple events, these spectral features were quantified and incorporated into our ripple detection algorithm (see STAR Methods).

(E) Normalized amplitude spectra for all detected real (top) and artifactual (bottom) ripple events (from S10, electrode 4, perception task runs 1–4); color map reflects percentage change in amplitude relative to the total signal mean. Yellow dashed line boxes indicate example ripples shown in (A)–(D). By identifying and removing artifactual ripples, mean ripple data display a clear ripple signature that is spectrally peaked and isolated in the ripple band.

(F) Ripple rates are shown for the example hippocampal recording (HP), and its surrogate data (HP(sg)), as well as an example cortical electrode (CX; see Figure S1 for electrode location) and its surrogate data (CX(sg)).

for any of the ripple attributes. These results suggest that ripple attributes are quite comparable between the two active cognitive tasks (perception and memory) and modestly different from the offline resting state, which shows slightly more pronounced ripple activity. Given the general stability of ripples across tasks, we next examined event-related changes in ripple rates, given the prior evidence of task modulation of ripple activity (Axmacher et al., 2008; Norman et al., 2019; Vaz et al., 2019).

Event-related ripples across cognitive tasks

To quantify event-related changes in ripple rates across tasks, detected ripple events were aligned to stimulus presentation conditions across all tasks (perception, memory, and resting). In addition, data from the memory task was separated into encoding/retrieval phases, while the rest task was separated into eyes open/closed phases. Event-related ripple events are shown for all tasks, subjects, electrodes, and trials in Figure 3. As noted above, and consistent with prior work, all tasks show clear evidence for ongoing ripple events. However, when considering event-related changes in ripple rates, no overt modulation was observed across tasks. This was true also when considering relative changes in ripple rate, in which the ripple rate time course was normalized by subtracting the mean ripple rate during the pre-stimulus baseline (500 ms) (Figures 3C, 3G, and 3K). While more modest in sample size, ripple rates were significantly higher for eyes closed, compared with eyes open (Wilcoxon rank sum test, $W = 52{,}513$, $p < 0.0001$), in the resting task. Behaviorally, we observed high accuracy for the 1-back perception task (mean hit rate 75.85%) and memory retrieval task (mean hit rate 81.57% and mean correct rejection rate 84.25%). Nonparametric Spearman correlation revealed no significant relationship between mean ripple rate and task accuracy (perception task: $\rho = 0.25$, $p = 0.42$; memory task: hit rate $\rho = 0.32$, $p = 0.21$ and correct rejection rate $\rho = 0.12$, $p = 0.64$). Overall, these data are consistent with the observations noted above, that hippocampal ripples occur at a stable rate during cognitive tasks, showing minimal task modulation and more sensitivity to general state changes (e.g., online versus offline states). Therefore, we next examined additional factors that may influence ripple events.

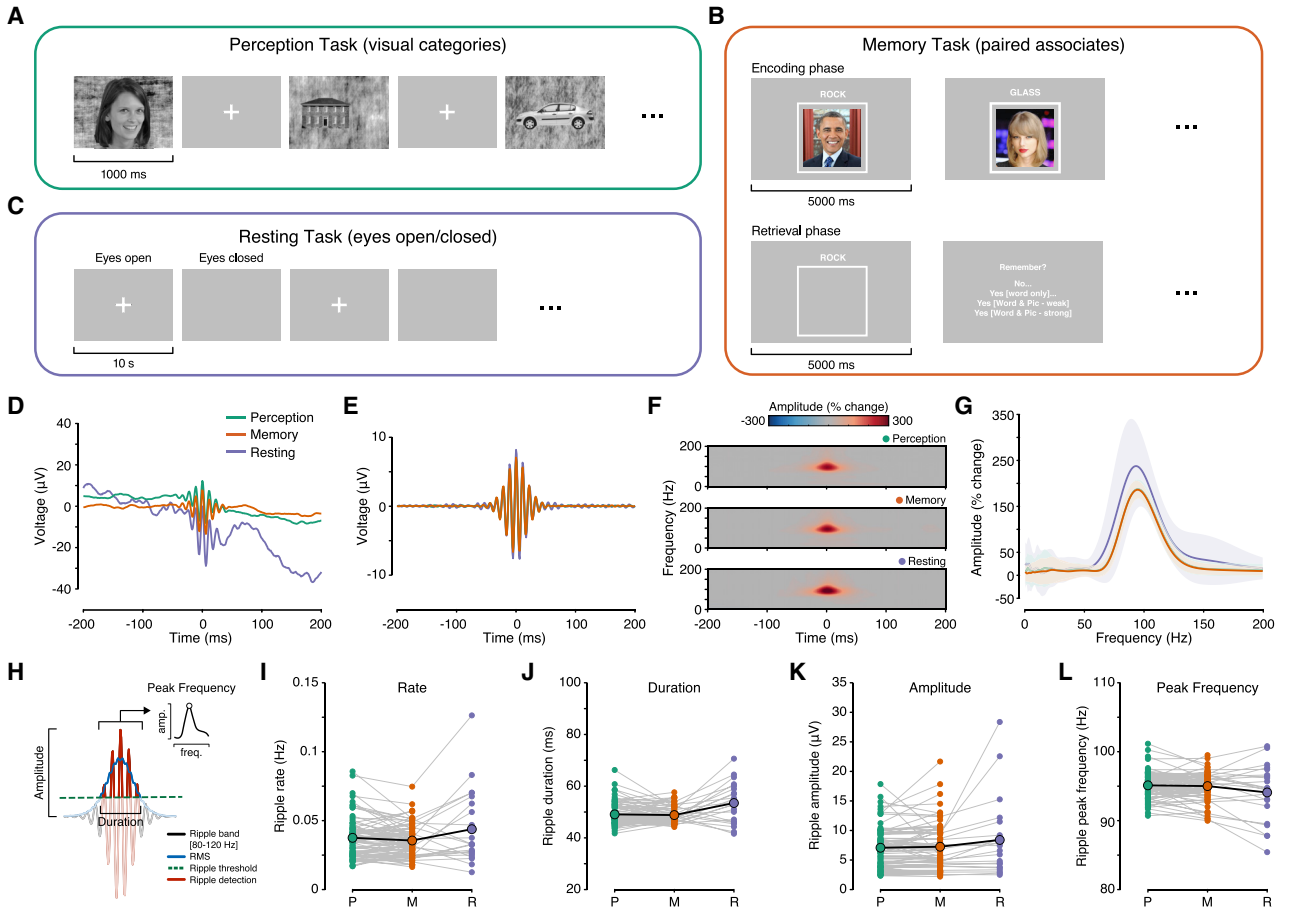

Figure 2. Ripple attributes across different cognitive tasks

(A) Perception task stimuli and experimental procedure. Grayscale images from 10 visual categories were presented for 1,000 ms with a random ISI of 1–1.5 s. Subjects had to provide a button press to indicate any 1-back stimulus repetition.

(B) Memory stimuli and experimental procedure. During the encoding phase, word-image pairs were presented for 5,000 ms with a self-paced inter-stimulus interval (ISI). During the retrieval phase, cue words were presented for 5,000 ms followed by a memory strength judgment. Subjects were required to encode word-face associations, and to retrieve the associated face image from presented word cues (including new cue words).

(C) Resting task experimental procedure. During the resting task, subjects alternated between 10-s periods of eyes open and eyes closed based on visual or auditory cues.

(D) Group-averaged ripple-triggered voltage trace for each task.

(E) Group-averaged ripple-band triggered voltage trace for each task.

(F) Group-averaged ripple-triggered spectrograms for each task; color maps reflect percentage change in amplitude relative to the total signal mean.

(G) Group-averaged normalized amplitude spectra (percentage change) for each task averaged over the detected ripple onset/offset window. Overall, hippocampal ripples were reliably detected across all 3 tasks, with highly comparable spectro-temporal properties.

(H) Schematic of ripple attribute quantification.

(I–L) Ripple attributes are shown for all of the subjects and electrodes across tasks: rate (I); duration (J), amplitude (K), and peak frequency (L). Statistical analysis revealed a significant main effect of task for rate, duration, and amplitude, in which these ripple attributes were significantly greater for the resting task compared with the memory and perception tasks (see Results: Ripple attributes across different cognitive tasks).

Ripple attributes across hemisphere, time, and other variables

To assess whether ripple attributes (rate, duration, amplitude, and peak frequency) were affected by other recording variables, we examined these attributes across recording sites, number of days postimplant surgery, and the time of day that the tasks were conducted (Figure 4). Consideration of these factors are important given the potential confound of pathophysiological activities and for exploring any putative functional effects of behavior. First, we compared ripple attributes between left and right hemispheres. Of the 82 included electrodes (Figure 4A for the anatomical location), 49 electrodes were identified in the left hippocampus. Similar to the group task results, ripple attributes did not show any large difference between left and right hemispheres (Figures 4B–4E). Extending our group linear mixed-effect analysis of ripple attributes, including hemispheres as an additional fixed effect and subject/electrode as random effects revealed no significant difference between left and right

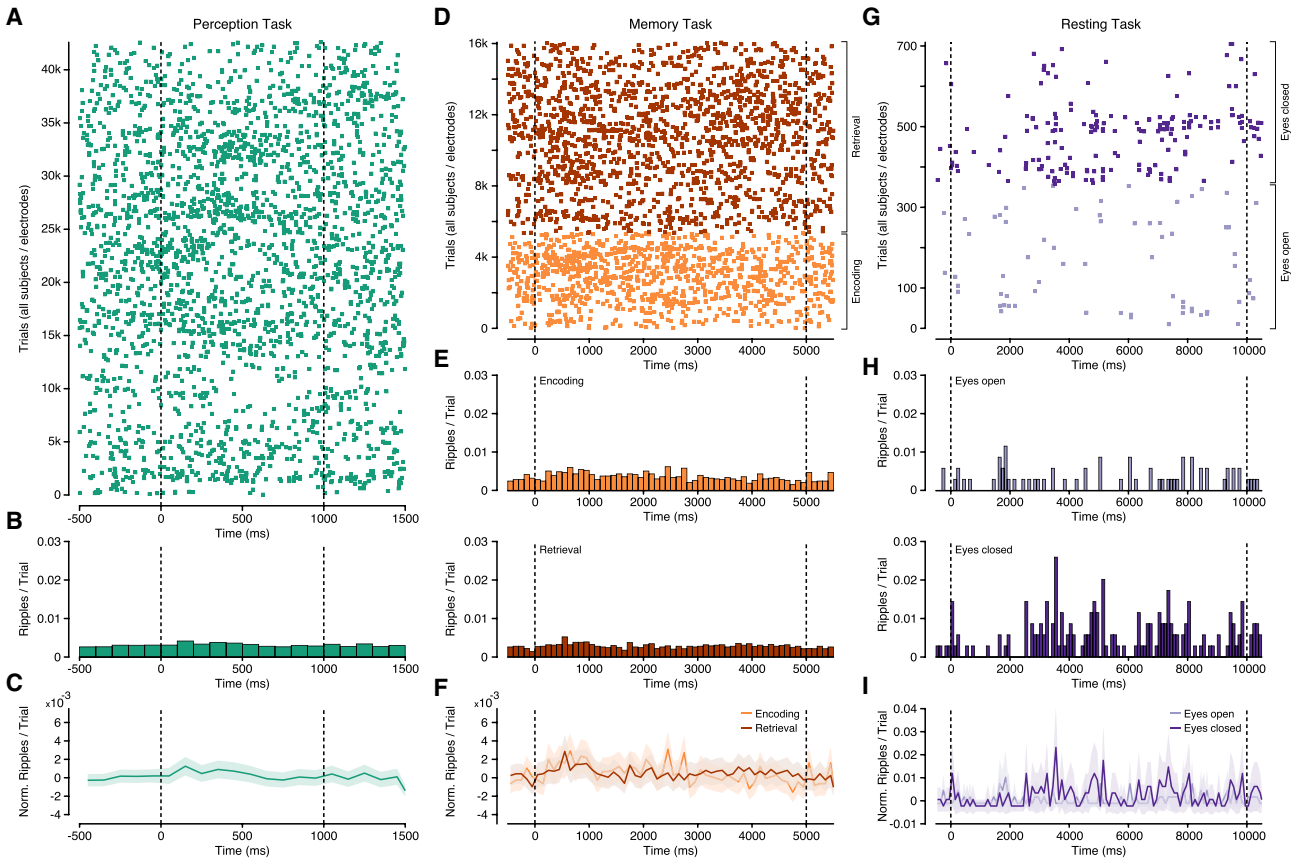

Figure 3. Event-related ripples across tasks for all subjects, electrodes, and trials

(A) Ripple events for the perception task (all electrodes × trials, n = 42,582); green markers indicate a single identified ripple event. Dashed lines indicate stimulus presentation period.

(B) Mean ripple rate across trials.

(C) Pre-stimulus baseline-corrected ripple rate across trials; error shading reflects 3 SEM.

(D) Ripple events for the memory task (all electrodes × trials, n = 16,065); markers indicate a single ripple event for encoding (orange) and retrieval (brown) trials. Dashed lines indicate stimulus presentation period.

(E) Mean ripple rates for encoding and retrieval trials.

(F) Pre-stimulus baseline-corrected ripple rates for encoding and retrieval; error shading reflects 3 SEM.

(G) Ripple events for the resting task (all electrodes × trials, n = 708); markers indicate a single ripple event for eyes open (light purple) and eyes closed (purple) trials. Dashed lines indicate start and end of the eyes open/eyes closed period.

(H) Mean ripple rates for eyes open and eyes closed trials.

(I) Pre-stimulus baseline-corrected ripple rates for eyes open and eyes closed; error shading reflects 3 SEM.

hemispheres in rate or duration, but a significant difference for amplitude and peak frequency. Specifically, using pairwise Tukey's range test, ripple amplitude was greater on the left hemisphere (left-right: $t(66) = 2.766$, $p = 0.0073$) and ripple peak frequency was greater on the right hemisphere (left-right: $t(88.5) = -3.904$, $p = 0.0002$). While significant, we note that these anatomical differences are modest in magnitude. Second, we examined the relationships between ripple attributes and days postimplant surgery. Most task recordings were performed between 1 and 5 days postimplantation, with ripple attributes being stable across days (Figures 4F–4I). Non-parametric Spearman correlation revealed no significant correlation between days postimplant and any of the ripple attributes (rate: $\rho = -0.05$, $p = 0.27$; duration: $\rho = -0.09$, $p = 0.06$; amplitude: $\rho = 0.01$, $p = 0.80$; frequency: $\rho = 0.07$, $p = 0.16$). Third, we examined the relationship between ripple attributes and the time-of-day recordings took place. Recordings were performed between 10 a.m. and 7 p.m., with the ripple attributes being stable throughout the day (Figures 4J–4M). Non-parametric Spearman correlation revealed no significant correlation between the time of day with any of the ripple attributes (rate: $\rho = 0.074$, $p = 0.11$; duration: $\rho = 0.07$, $p = 0.14$; amplitude: $\rho = 0.02$, $p = 0.59$; frequency: $\rho = -0.09$, $p = 0.05$). In addition to recording variables, we assessed whether ripple attributes were affected by the age and sex of the subjects. Extending our group linear mixed-effect analysis of ripple attributes, including age and sex as additional fixed effects and subject/electrode as random effects revealed no significant main effect of age or sex. These results suggest that hippocampal ripples and their attributes do not meaningfully differ between hemisphere, sex, or age, and are stable across and within days.

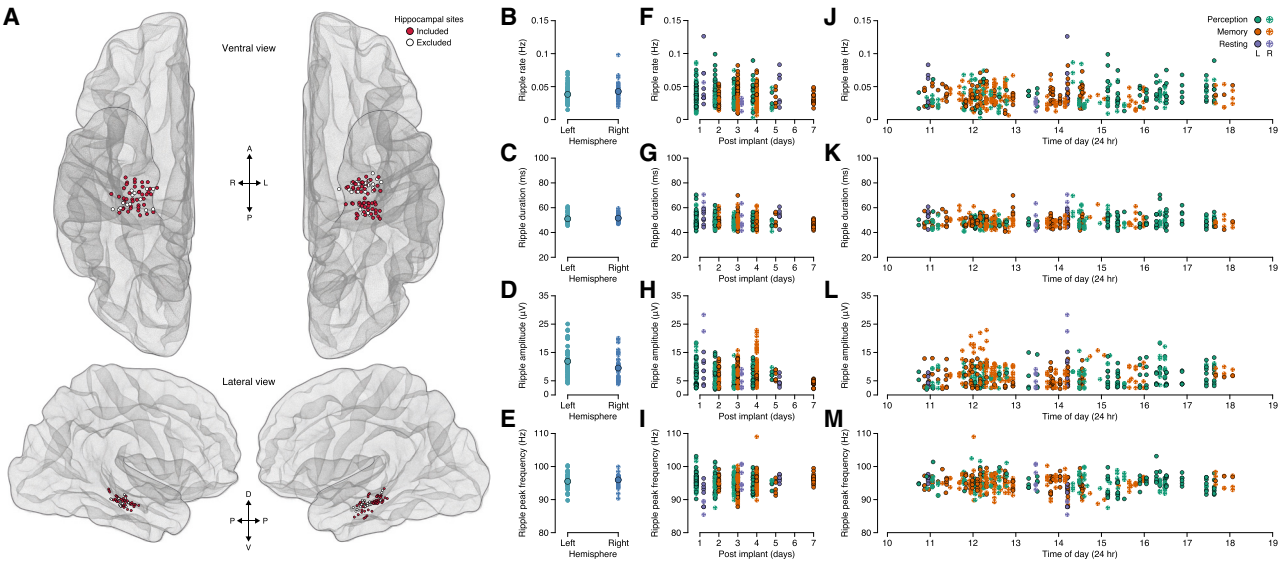

Figure 4. Ripple attributes across hemisphere and time

(A) Anatomical location of identified hippocampal electrodes from all subjects, normalized to Montreal Neurological Institute (MNI) space. Included electrodes, which passed a selection criterion, are shown in red, with excluded electrodes shown in white (see STAR Methods). Ripple attributes of rate, duration, amplitude, and peak frequency are shown as a function of anatomy and time.

(B–E) Ripple attributes (rate, duration, amplitude, peak frequency) are shown for all electrodes, averaged across tasks, from the left and right hemispheres.

(F–I) Ripple attributes (rate, duration, amplitude, peak frequency) are shown for each electrode, task (perception, memory, resting), and hemisphere (left/right) as a function of the days postelectrode implantation.

(J–M) Ripple attributes (rate, duration, amplitude, peak frequency) are shown for each electrode, task (perception, memory, resting), and hemisphere (left/right) as a function of the time of day that recordings were performed. Overall, hippocampal ripple attributes were similar between hemispheres and stable across and within days.

Such findings suggest a limited impact of pathophysiological factors affecting overall ripple statistics. In turn, they also suggest that ripples occur at a low and regular rate throughout the waking day and do not appear to show any pronounced modulation specific to memory behavior. Consistent with a large literature, ripple rates are expected to be more pronounced during offline states. While we observed modest evidence for this during the resting task, offline sleep states have shown the most pronounced effects. In addition, we examined only one perceptual task that included faces, scenes, and objects not unlike our memory paradigm. Therefore, in an attempt to empirically consider these factors, we examined ripple attributes across additional perception tasks as well as during sleep.

Ripple attributes across multiple task and state conditions

In one subject (S12), we carried out three additional perception tasks (perception-grating, perception-color, and perception-color obj.), as well as recording one night of sleep to assess how task and state conditions influenced ripple attributes. We sought to examine (1) whether ripple attributes were comparable among cognitive tasks and (2) whether ripple attributes during sleep, a pronounced offline state, differed from other cognitive states within a subject. As shown in Figure 5, hippocampal ripples were readily detected across all six tasks and three sleep stages, displaying highly similar electrographic signatures, with the only exception for NREM sleep (Figures 5B–5E). Notably, in the subject-averaged ripple-triggered raw voltage trace plot (Figure 5B), ripples recorded during NREM sleep were nested in a slower oscillation that displayed large voltage deviation compared to other cognitive tasks and sleep stages. In addition, the normalized amplitude spectra for NREM sleep ripples (Figure 5E) showed a higher amplitude percentage change, but a lower-frequency, ripple band peak compared to other cognitive tasks and sleep stages. These observations illustrate a clear difference between NREM sleep ripples and other tasks and sleep stage ripples. Therefore, to compare across tasks and sleep stages, we carried out linear mixed-effects analysis modeling ripple attributes with task/sleep stage as a fixed effect and treating electrode as a random effect. Satterthwaite approximations to test the significance of the model coefficients revealed a significant main task/sleep stage for rate, duration, amplitude, and peak frequency. Using a pairwise Tukey's range test, with p value adjustment for comparing a family of nine estimates (perception, memory, resting, perception-grating, perception-color, perception-color obj., Awake, REM sleep, and NREM sleep), we compared the ripple attributes among tasks and sleep stages (summarized results in Table S2). Specifically, the ripple rate was significantly higher for NREM sleep than other tasks and sleep stages; the ripple duration was significantly longer for NREM sleep than memory, awake, and REM sleep; the ripple amplitude was significantly greater for NREM sleep than other tasks and REM sleep, but not for awake; and the ripple peak frequency for NREM sleep was significantly lower than other tasks

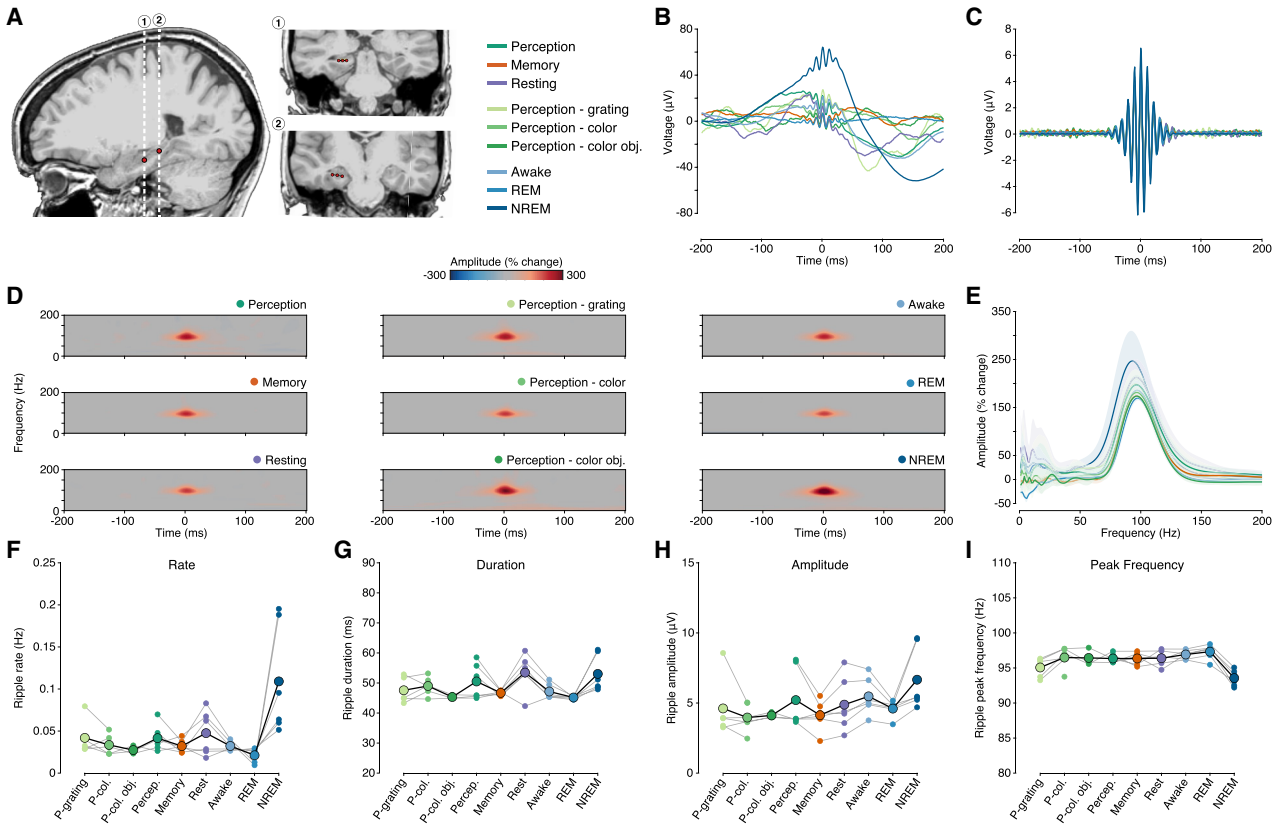

Figure 5. Ripple attributes across task and sleep states

(A) Anatomical location of hippocampal electrodes (n = 6) in subject S12 for 2 stereo iEEG depth probes. Sagittal view (left) shows longitudinal position of each probe, with the white dashed lines indicating the respective coronal slices (right; ① and ②).

(B) Subject-averaged ripple-triggered raw voltage trace for each task and sleep stage.

(C) Subject-averaged ripple-triggered voltage trace within the ripple band for each task and sleep stage.

(D) Subject-averaged ripple-triggered spectrograms for each task and sleep stage; color maps reflect percentage change in amplitude relative to the total signal mean.

(E) Subject-averaged normalized amplitude spectra (percentage change) for each task and sleep stage, estimated over the detected ripple onset/offset window. Overall, hippocampal ripples were reliably detected across all 6 tasks and 3 sleep stages, with highly comparable spectro-temporal properties. However, it is noticeable that ripple-triggered activity during NREM is uniquely nested within a slower frequency oscillation (see Figure S2), as previously observed (Staresina et al., 2015).

(F–I) Ripple attributes are shown for all electrodes across tasks and sleep stages: rate (F), duration (G), amplitude (H), and peak frequency (I) (small circles reflect electrodes, large circles reflect means). For some tasks and electrodes, no ripples were detected. Statistical analysis revealed a significant main effect of task and sleep stage, whereby ripple attributes recorded during NREM were significantly different from the other tasks and sleep stages (see Results and Table S2).

and sleep stages, except for the perception-grating task. Overall, ripple attributes during NREM sleep were distinctly different from other cognitive states and sleep stages. Further analysis of the NREM sleep data revealed a nesting of hippocampal ripples, in which the average ripple-triggered raw voltage displayed a clear alignment to larger slow oscillations (see Figure S2). Furthermore, the peak ripple-triggered spectrogram showed that narrow band ripple activity was accompanied by increased amplitude in the spindle and slow oscillation frequency ranges. This putative nesting effect was further confirmed by phase-amplitude coupling analysis, in which we explored the comodulation of low-frequency (2–9 Hz) phase and high-frequency (10–170 Hz) amplitudes. This analysis revealed a clear coupling of the slow oscillation (<4 Hz) phase with spindle and ripple band amplitude (Figure S2). These results suggest that ripples detected with our approach from NREM sleep data are highly comparable to previously published human studies (Staresina et al., 2015).

Ripple attributes during performance and switches between more complex cognitive tasks

Across a variety of separate cognitive tasks, we observed a high stability in ripple event attributes. However, we did not test the stability of ripple event attributes during the active switching of cognitive states (i.e., within task switching). It is possible that active switching between "memory," "non-memory"/"attentional," or "rest" task conditions affects ripple activity differently from the separate performance of these tasks. We probed perception/attention and episodic memory using basic task designs (e.g., item-based paired associates). This approach may be a weaker means for testing hippocampal

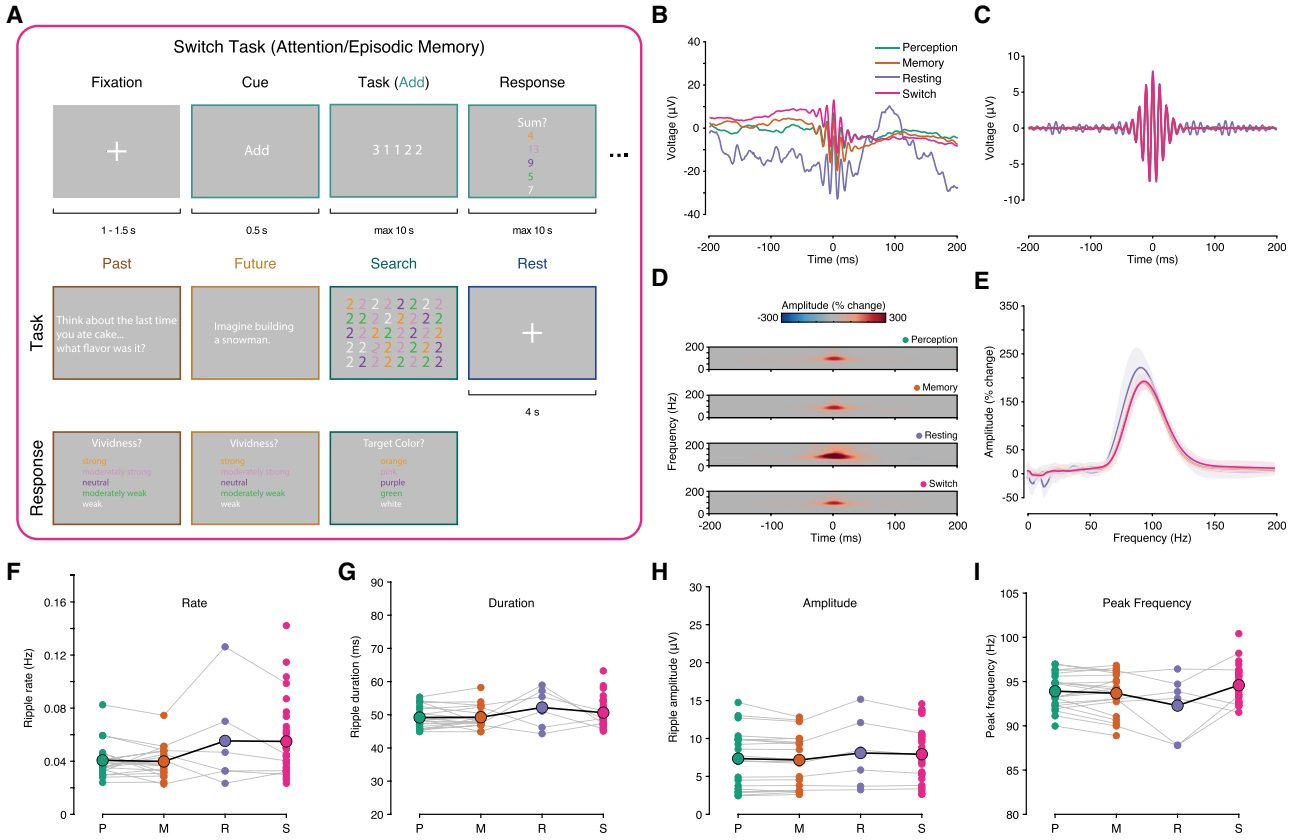

Figure 6. Ripple attributes and attention/episodic memory switch task

(A) Switch task stimuli and experimental procedure. Each task trial started with a jittered 1–1.5 s fixation and task cue presented for 500 ms, indicating the trial condition. Then, the task question was presented for a maximum of 10 s (except for rest condition, 4 s) followed by a response screen.

(B) Subgroup (S10, S11, S15, and S18)-averaged ripple-triggered voltage trace for perception, memory, resting, and switch tasks.

(C) Subgroup-averaged ripple-band triggered voltage trace for each task.

(D) Subgroup-averaged ripple-triggered spectrograms for each task; color maps reflect percentage change in amplitude relative to the total signal mean.

(E) Subgroup-averaged normalized amplitude spectra (percentage change) for each task averaged over the detected ripple onset/offset window. Overall, hippocampal ripples were reliably detected across all 4 tasks, with highly comparable spectro-temporal properties.

(F–I) Ripple attributes are shown for the subgroup and electrodes across tasks: rate (F); duration (G), amplitude (H), and peak frequency (I). Overall, hippocampal ripple attributes were similar among 4 cognitive tasks.

ripple activity, given the simplicity of task demands. Therefore, in a final experiment, 4 subjects (S10, S11, S15, and S18) performed an attention (search, add), memory (past, future) and rest (fixation) switch task (see STAR Methods; Figure 6). Importantly, trials (attention, memory, rest) occurred in random order, with memory conditions probing past and future autobiographical events. As shown in Figure 6, the switch task showed similar ripple attributes to other experiments performed. Group linear mixed-effects analysis was performed, modeling ripple attributes with conditions as a fixed effect and subject/electrode as a random effect. Satterthwaite approximations to test the significance of the model coefficients revealed no significant main effect of task for rate and duration, but a significant main effect for amplitude and peak frequency. Specifically, using the pairwise Tukey's range test, p value adjusted for comparing a family of 4 estimates, ripple amplitude was greater in resting than the other 3 tasks (resting-memory: $t(48.2) = 8.158$, $p < 0.0001$, resting-perception: $t(48.2) = 5.313$, $p < 0.001$, and resting-switch: $t(48.3) = 3.583$, $p = 0.0043$) and was greater in switch than perception and memory tasks (switch-memory: $t(48.4) = 4.214$, $p = 0.0006$, switch-perception: $t(48.4) = 2.833$, $p = 0.033$). Therefore, for the subjects who performed the switch task, ripple attributes were relatively stable across the four tasks performed.

Event-related ripples are specifically enhanced for autobiographical thought

Strikingly, when comparing ripple attributes across conditions within the switch task, we observed a clear increase in ripple rates specifically during the autobiographical episodic memory conditions (past and future events; Figure 7). To test this effect, group linear mixed-effects analysis modeling ripple attributes with condition as a fixed effect and subject/electrode as random effects was performed. Satterthwaite approximations to test the significance of the model coefficients revealed a significant main effect of conditions on ripple rate. Only the past and future

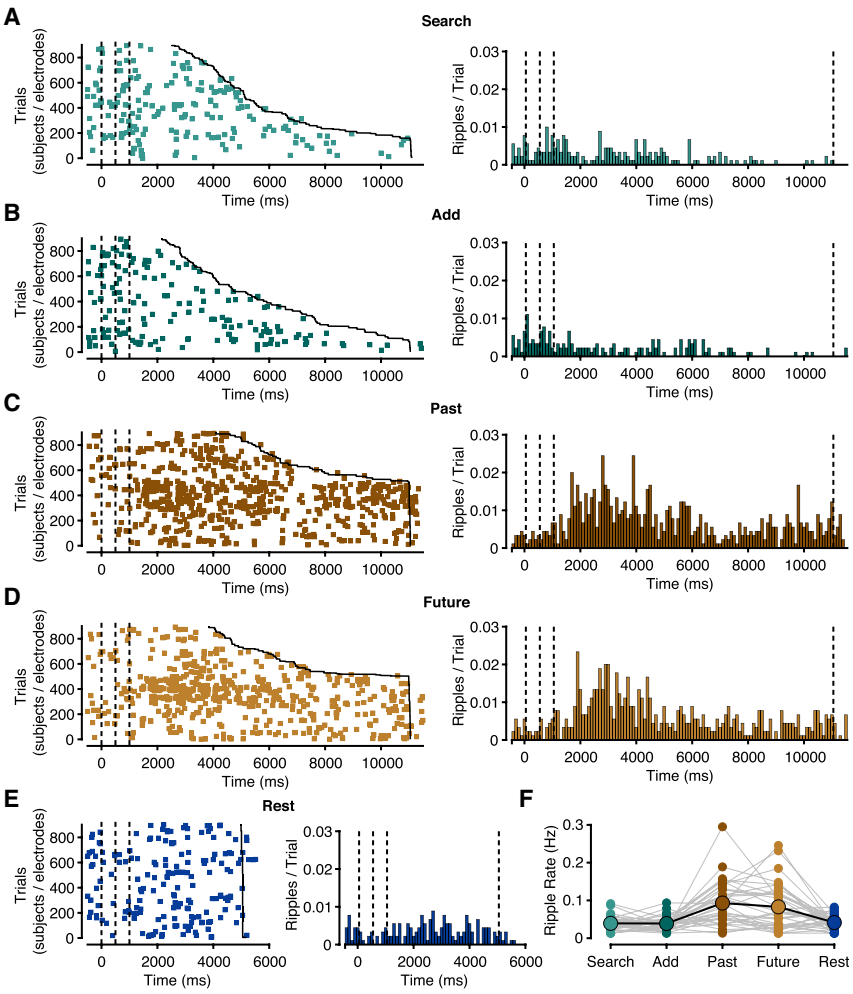

Figure 7. Event-related ripples for switch task

Event-related ripples across 5 conditions of the switch task for subjects (S10, S11, S15, S18) and all of their electrodes and trials.

(A–E) Ripple events raster (left) and mean ripple/trial (right) for the search (A), add (B), past (C), future (D), and rest (E) conditions (all electrodes × trials, n = 900, each marker indicates a single identified ripple event). Events are sorted by trial response time (shortest to longest). Dashed lines indicate fixation (time 0), cue onset (time 500 ms), task stimulus presentation onset (time 1,000 ms), and offset (maximum time, 11,000 ms). Solid lines indicate the end of the trials.

(F) Ripple rates are shown for all electrodes across 5 conditions. Statistical analysis revealed a significant main effect of condition, in which ripple rates were significantly greater for the past and future conditions compared with the search, add, and rest conditions (see Results and Table S3).

conditions, across all conditions, showed a clear event-related modulation of ripple rates (summarized in Table S3). Importantly, we note that while task modulated, ripple rates remained low frequency (mean rate past: 0.061 Hz; future: 0.059 Hz), with event-related increases being "late" in onset (peak rate ~2,900 ms postonset of the trial cue). These findings suggest a high consistency of ripple event attributes across a wide range of tasks, which are primarily modulated by changes in state, but also may be particularly sensitive to more hippocampal-dependent episodic autobiographical thought.

DISCUSSION

Using direct intracranial recordings from the human hippocampus, we quantified hippocampal ripple attributes across different cognitive tasks, sleep stages, recording hemispheres, and potential pathophysiological factors. Our results highlighted the general stability of ripples attributes across cognitive tasks. Ripple rate, duration, amplitude, and frequency were comparable between perception and memory tasks; however, they differed from offline resting conditions, most notably NREM sleep and, importantly, more complex autobiographical memory retrieval processes. Moreover, ripple attributes were generally stable between recording hemispheres, throughout the time of day and proximity to electrode implantation date.

Hippocampal ripples are short bursts of high-frequency activity (80–120 Hz in humans) that have been linked to memory consolidation, specifically the reactivation or replay of memory content during offline states such as rest or NREM sleep (Diekelmann and Born, 2010; Joo and Frank, 2018; Klinzing et al., 2019; Liu et al., 2019). More recently, hippocampal ripples have been recorded during awake online states, specifically during episodic memory tasks (Norman et al., 2019; Vaz et al., 2019). While it is important to examine the functional significance of ripples in facilitating memory encoding and retrieval, it is unclear whether ripples occur in other cognitive tasks or how their properties are modulated by task demands. Work in rodents exploring the differences across brain states has demonstrated that the occurrence of ripples is much lower during awake compared to prolonged immobility or sleep (Buzsáki, 2015; Joo and Frank, 2018). Furthermore, ripple attributes such as amplitude, duration, and peak frequency have been reported to differ between awake exploration, sleep and rest (Buzsáki, 2015), which could be important neural markers for cognitive processes. Here, we examined ripple attributes across our three main tasks, two cognitive tasks, and offline resting (Figure 2), and then additionally during a switch task (Figure 6). These tasks were chosen so as to directly compare ripples found during episodic-memory (memory) versus non-episodic-memory tasks (perception). We also included an offline awake resting condition for comparing online and offline brain states. In general, we found that ripple attributes were stable between awake cognitive tasks regardless of the engagement in episodic memory behavior. However,

during resting states, ripples showed a higher occurrence rate and were longer in duration and larger in amplitude. Initially, these data suggest that hippocampal ripples were not increased during episodic-memory behavior, given that ripple attributes were comparable between episodic and non-episodic tasks. However, we found that more complex autobiographical probes for past and future scenarios did enhance ripple rates. Overall, the largest difference in ripple attributes were observed during NREM sleep in which ripple rate was higher, with longer duration and greater amplitude but slower peak frequency in contrast to any other cognitive task or sleep stages. This result is in line with the idea that hippocampal ripples play a pivotal role in NREM sleep-mediated memory consolidation (Klinzing et al., 2019). Importantly, we note the limitation that sleep data were examined in only one subject and that only a subset of subjects (n = 3) performed the resting task.

While we reliably detected hippocampal ripples across all tasks, some aspects of ripple attributes differ from prior work. First, ripple rates detected during cognitive tasks were much lower compared to prior work. For example, recent work by Vaz et al. (2019) reported a mean ripple rate of 0.21 ± 0.02 Hz across participants during an episodic task, and soon after, Norman et al. (2019) reported ripple rates of 0.41 Hz across all of the experimental conditions; in contrast, our averaged ripple rate across the three main tasks was an order of magnitude smaller, at 0.037 ± 0.013 Hz. Second, prior studies have highlighted that increased ripple rates during encoding and retrieval were indicative of successful memory (Norman et al., 2019; Vaz et al., 2019). In our first set of experiments, we did not observe any clear event-related change in ripple rate in the memory or perception task, although difference between eyes open and eyes closed were observed for the resting task. However, in the switch task autobiographical memory conditions (past / future events), we observed consistent increases in ripple rates across subjects (Figure 7).

Several factors may account for these differences. One important consideration is the anatomical locations of ripple recording sites. For example, Vaz et al. (2019) examined ripple events from the MTL cortical structures, including the entorhinal cortex and the parahippocampal gyrus, but not the hippocampus. Consequently, higher ripple rates may be present in neocortical structures, although it is typically viewed that the hippocampus is the key generator of ripple activity (Axmacher et al., 2008; Buzsáki, 2015). However, Norman et al. (2019) recently reported similar findings, which included direct hippocampal recordings, observing higher rates as noted above. Therefore, while ripple events have been historically viewed as a hippocampal phenomenon, they may be observed in the neocortex, and with higher rates or occurrence, but such factors do not fully account for differences with the present study. Finally, in our findings, event-related increases in ripple rates were observed only for the autobiographical memory conditions and not the paired associate's memory task. This increase in rate is likely linked to the more complex, event-based, and multi-feature nature of cued autobiographical probes, requiring a higher demand of hippocampal function (Schacter et al., 2007). Importantly, while there is a significant increase in ripple rates during episodic autobiographical memory retrieval, ripple rates remained low when compared to prior studies.

Another critical factor is the ripple detection method used. Given that direct hippocampal recordings in human subjects are collected from individuals undergoing invasive monitor as part of their treatment for refractory epilepsy, many studies have expressed concerns for reliable and genuine ripple detection (Jiang et al., 2020). Particularly, many electrodes localized in the hippocampus are proximal to or within seizure onset zones, which generate high-frequency oscillations (HFOs; 80–500 Hz) and inter-ictal epileptic spikes (Jacobs et al., 2012). Therefore, simple ripple detection methods may be prone to false positives (see Figure 1 for examples). To remedy this possible false detection, prior studies have used different validation methods, including visual inspection of randomly sampled data (Vaz et al., 2019), and excluding simultaneously detected events on multiple channels, or proximity of ripple event occurrence to pathological events (Norman et al., 2019), as well as other steps for artifact rejection.

To reliably detect genuine hippocampal ripples, we applied additional time-frequency criteria to reject potential false positives after initial identification via ripple band threshold-based detection. First, we included a conservative duration rejection threshold of 38 ms, which corresponds to 3 cycles at 80 Hz, the lower bound of the ripple band frequency. This duration threshold ensured that the detected signal is a sustained oscillatory event rather than a single isolated transient signal change such as an inter-ictal spike or a recording noise. It is worth noting that Vaz et al. (2019) reported 34 ms as their average duration recorded from MTL electrodes, with an estimated range of 25–60 ms. Therefore, our approach would have excluded some of the short-duration ripples reported. However, it is important to point out that in a follow-up analysis, Vaz et al. (2019) excluded short-duration ripples (25–30 ms) and still found significant memory effects. Second, we included a ripple spectra rejection method in which events that did not exhibit a stereotypical ripple spectra profile were excluded, consistent with some prior sleep studies (Jiang et al., 2019, 2020; Ngo et al., 2020). This approach allowed us to look beyond the typical bandpass filtered ripple band data. Examining the wide band spectral change enabled us to identify low-frequency noise, broadband transients, or HFOs that could be misidentified as a ripple event. These criteria likely account for the lower ripple event rates observed in the present study. Importantly, we note that this approach may be too conservative, such that our false negative rate may be inflated. It is important to note that we also excluded electrodes if the spectral-based rejection rate was >30% of all identified ripple events. This step aimed to exclude both noisy electrodes, not identified in early stages of processing, and the erroneous creation of low rate recordings. While establishing ground truth for ripples rates within the human hippocampus can be difficult, we believe that our reported rates fall within an appropriate range. Central to this conclusion is that prior work in the human hippocampus focused on NREM sleep, in which ripple rates are thought to be maximal, typically report rates within the range of 0.1–0.5 Hz (Jiang et al., 2020). In addition, a subset of these sleep focused studies reported ripple rates during awake states with a range of 0.01–0.1 Hz (Jiang et al., 2020). These ripple rate ranges

are more comparable to our observations. As shown in Figure 5, when applying our methods to NREM sleep data, we observed similar ripple rates, which, importantly, are on average larger than most task conditions examined. Additional analysis of NREM sleep data revealed a ripple-spindle-slow oscillation nesting effect, as shown in Figure S2, which is also consistent with prior human hippocampal sleep recordings (Helfrich et al., 2019; Staresina et al., 2015). Moreover, a relatively low ripple occurrence was also reported by prior work in non-human primates. For example, Logothetis et al. (2012) examined hemodynamic neuroimaging responses time locked to electrophysiological hippocampal ripple events in the macaque. Using ripple band threshold detection as well as spectral selection, similar to the present study, these authors reported ripple rates of 5.6/min (0.09 Hz) during unanesthetized spontaneous recordings. In addition to similar rates of ripple events, ripple duration and peak frequency in the macaque were highly similar to our observations in the human (Logothetis et al., 2012). These low rates in the macaque may be related to a lack of task engagement; however, similarly low rates have been observed in the macaque hippocampus during perceptual memory tasks (Leonard and Hoffman, 2017; Leonard et al., 2015). For example, Leonard and colleagues observed low-rate hippocampal ripple events during complex visual scene viewing (maximum rate ~1.12/min, 0.019 Hz), which showed a slow drifting increase during visual search (Leonard et al., 2015) that was subsequently shown to be enhanced for repeated versus novel scenes (Leonard and Hoffman, 2017). Such slow changes in ripple rate are similar to our lack of rapid event-related changes in ripple rates and suggest that modulations in rate occur over slower timescales. This view is consistent with prior observations in the rodent showing a tight anticorrelated coupling between slow changes in arousal states (i.e., pupil dilation) and hippocampal ripple rate (McGinley et al., 2015a, 2015b). In addition, it is consistent with ripple events occurring via intrinsic mechanisms, rather than externally driven stimulus events (Kay and Frank, 2019). In summary, our findings replicate prior observations of online hippocampal ripple events, but differ in the mean rate of ripples and their task selectivity. While these differences may be related to the detection methods used, our observations are consistent with prior sleep studies in humans and other non-human primate studies examining hippocampal ripple activity (Helfrich et al., 2019; Jiang et al., 2020; Leonard et al., 2015; Logothetis et al., 2012; Ngo et al., 2020).

In addition to examining task demands and brain state modulation of ripple attributes, we considered other factors that may influence ripple rate. We observed no statistically significant difference in ripple attributes between hemispheres, both in aggregate and when considering specific tasks. Also, we examined whether our observations were potentially biased by patient state factors. To do so, we quantified ripple attributes as a function of the days postelectrode implantation and as a function of the time of day that recordings were performed. However, we observed no correlation of ripple attributes with either chronological variable, for a reasonable spread of days postimplantation (1–7 days) and time of day (~11 a.m.–6 p.m.). These findings suggest that hippocampal ripple attributes are stable throughout the day, making our comparisons across tasks unlikely to be confounded by these factors. More generally, these observations further support the notion of ripple events being stable across a host of conditions, and being most sensitive to overt behavioral state changes (e.g., online versus offline).

Why might hippocampal ripples occur with such stability throughout waking states? One natural hypothesis would be that ongoing and sparse hippocampal ripple events aid in establishing latent memory traces, consistent with two-stage models of systems consolidation (Dudai et al., 2015; Klinzing et al., 2019; Kumaran et al., 2016). This view may lead to evidence that ripple events are modulated by factors associated with subsequent memory behavior, as previously observed; however, this was not strongly supported by our findings. It is important to note that while subjects did perform an explicit episodic memory task, this is not a unique period of putative memory encoding, as we expect subjects to later recall performing other tasks as a simple consequence of their own autobiographical memory. It will therefore be important for future studies to carefully quantify key behavioral factors that influence hippocampal ripple rates and the veracity of their neocortical counterparts. In doing so, continued convergence of evidence across species can be obtained to further elucidate the mechanisms of memory consolidation. In addition, ripples have been identified as the most prominent self-organized event in the hippocampus and may reflect the default pattern of hippocampal circuits. Therefore, changes in ripple attributes could be indicative of brain states (Buzsáki, 2015; Kay and Frank, 2019). This view may lead to evidence that ripple events are modulated by factors associated with states of the brain, such as arousal, as noted above. The stable ripple rates we observed could be a result of overall similar arousal during these tasks. While we did not directly assess the arousal levels of our participants, the crude separation of online and offline tasks did reveal changes in ripple attributes associated with brain state.

In conclusion, our findings integrate and extend prior work in the human, the non-human primate, and the rodent hippocampus to suggest that ripple events are relatively stable across cognitive tasks. Ripple events were not unique to episodic-memory behavior, occurring with similar attributes during other perceptual tasks; however, their enhancement only occurred for more rich autobiographical memory processes and offline brain states. Such findings add growing support to the view that hippocampal ripples serve as an internally generated and state-dependent mechanism for establishing, and subsequently strengthening, memory traces in the mammalian brain.

STAR★METHODS

Detailed methods are provided in the online version of this paper and include the following:

- KEY RESOURCES TABLE
- RESOURCE AVAILABILITY
  - Lead contact
  - Materials availability
  - Data and code availability
- EXPERIMENTAL MODEL AND SUBJECT DETAILS
  - Human subjects

SUPPLEMENTAL INFORMATION

Supplemental information can be found online at https://doi.org/10.1016/j.celrep.2021.109304.

ACKNOWLEDGMENTS

The authors thank Hong-Viet Ngo and Bernhard Staresina for assisting with sleep staging neural data. This work was supported by NIH grants R01EY023336 (to D.Y.), R01MH106700 (to S.A.S.), and R01MH116914 (to B.L.F.). S.A.S. is also supported by the McNair Foundation and Dana Foundation.

AUTHOR CONTRIBUTIONS

Conceptualization and methodology, Y.Y.C. and B.L.F.; investigation and resources, Y.Y.C., B.L.F., L.A.-G., E.B., D.Y., and S.A.S.; data curation and software, Y.Y.C., B.L.F., and E.B.; writing and visualization, Y.Y.C. and B.L.F.

DECLARATION OF INTERESTS

The authors declare no competing interests.

Received: November 11, 2020
Revised: April 2, 2021
Accepted: June 3, 2021
Published: June 29, 2021

REFERENCES

Axmacher, N., Elger, C.E., and Fell, J. (2008). Ripples in the medial temporal lobe are relevant for human memory consolidation. Brain *131*, 1806–1817.

Bartoli, E., Bosking, W., Chen, Y., Li, Y., Sheth, S.A., Beauchamp, M.S., Yoshor, D., and Foster, B.L.. (2019). Functionally distinct gamma range activity revealed by stimulus tuning in human visual cortex. Curr. Biol. *29*, 3345–3358.e7.

Bates, D., Maechler, M., Bolker, B., Walker, S., Christensen, R.H.B., Singmann, H., and Dai, B. (2014). lme4: Linear mixed-effects models using Eigen and S4 (Version 1.1-7). https://cran/r-project org/web/packages/lme4/index html.

Bragin, A., Engel, J., Jr., Wilson, C.L., Fried, I., and Buzsáki, G. (1999). High-frequency oscillations in human brain. Hippocampus *9*, 137–142.

Brainard, D.H. (1997). The Psychophysics Toolbox. Spat. Vis. *10*, 433–436.

Buzsáki, G. (2015). Hippocampal sharp wave-ripple: a cognitive biomarker for episodic memory and planning. Hippocampus *25*, 1073–1188.

Canolty, R.T., Edwards, E., Dalal, S.S., Soltani, M., Nagarajan, S.S., Kirsch, H.E., Berger, M.S., Barbaro, N.M., and Knight, R.T. (2006). High gamma power is phase-locked to theta oscillations in human neocortex. Science *313*, 1626–1628.

Chen, Z., and Wilson, M.A. (2017). Deciphering Neural Codes of Memory during Sleep. Trends Neurosci. *40*, 260–275.

Cox, R.W. (1996). AFNI: software for analysis and visualization of functional magnetic resonance neuroimages. Comput. Biomed. Res. *29*, 162–173.

Dale, A.M., Fischl, B., and Sereno, M.I. (1999). Cortical surface-based analysis. I. Segmentation and surface reconstruction. Neuroimage *9*, 179–194.

Diekelmann, S., and Born, J. (2010). The memory function of sleep. Nat. Rev. Neurosci. *11*, 114–126.

Dudai, Y., Karni, A., and Born, J. (2015). The Consolidation and Transformation of Memory. Neuron *88*, 20–32.

Groppe, D.M., Bickel, S., Dykstra, A.R., Wang, X., Mégevand, P., Mercier, M.R., Lado, F.A., Mehta, A.D., and Honey, C.J. (2017). iELVis: an open source MATLAB toolbox for localizing and visualizing human intracranial electrode data. J. Neurosci. Methods *281*, 40–48.

Helfrich, R.F., Lendner, J.D., Mander, B.A., Guillen, H., Paff, M., Mnatsakanyan, L., Vadera, S., Walker, M.P., Lin, J.J., and Knight, R.T. (2019). Bidirectional prefrontal-hippocampal dynamics organize information transfer during sleep in humans. Nat. Commun. *10*, 3572.

Iber, C.; American Academy of Sleep Medicine (2007). The AASM Manual for the Scoring of Sleep and Associated Events: Rules, Terminology and Technical Specifications (American Academy of Sleep Medicine).

Jacobs, J., Staba, R., Asano, E., Otsubo, H., Wu, J.Y., Zijlmans, M., Mohamed, I., Kahane, P., Dubeau, F., Navarro, V., and Gotman, J. (2012). High-frequency oscillations (HFOs) in clinical epilepsy. Prog. Neurobiol. *98*, 302–315.

Jiang, X., Gonzalez-Martinez, J., and Halgren, E. (2019). Coordination of Human Hippocampal Sharpwave Ripples during NREM Sleep with Cortical Theta Bursts, Spindles, Downstates, and Upstates. J. Neurosci. *39*, 8744–8761.

Jiang, X., Gonzalez-Martinez, J., Cash, S.S., Chauvel, P., Gale, J., and Halgren, E. (2020). Improved identification and differentiation from epileptiform activity of human hippocampal sharp wave ripples during NREM sleep. Hippocampus *30*, 610–622.

Joo, H.R., and Frank, L.M. (2018). The hippocampal sharp wave-ripple in memory retrieval for immediate use and consolidation. Nat. Rev. Neurosci. *19*, 744–757.

Kay, K., and Frank, L.M. (2019). Three brain states in the hippocampus and cortex. Hippocampus *29*, 184–238.

Kiani, R., Esteky, H., Mirpour, K., and Tanaka, K. (2007). Object category structure in response patterns of neuronal population in monkey inferior temporal cortex. J. Neurophysiol. *97*, 4296–4309.

Klinzing, J.G., Niethard, N., and Born, J. (2019). Mechanisms of systems memory consolidation during sleep. Nat. Neurosci. *22*, 1598–1610.

Kumaran, D., Hassabis, D., and McClelland, J.L. (2016). What Learning Systems do Intelligent Agents Need? Complementary Learning Systems Theory Updated. Trends Cogn. Sci. *20*, 512–534.

Lancaster, G., Iatsenko, D., Pidde, A., Ticcinelli, V., and Stefanovska, A. (2018). Surrogate data for hypothesis testing of physical systems. Phys. Rep. *748*, 1–60.

Leonard, T.K., and Hoffman, K.L. (2017). Sharp-Wave Ripples in Primates Are Enhanced near Remembered Visual Objects. Curr. Biol. *27*, 257–262.

Leonard, T.K., Mikkila, J.M., Eskandar, E.N., Gerrard, J.L., Kaping, D., Patel, S.R., Womelsdorf, T., and Hoffman, K.L. (2015). Sharp Wave Ripples during Visual Exploration in the Primate Hippocampus. J. Neurosci. *35*, 14771–14782.

Liu, Y., Dolan, R.J., Kurth-Nelson, Z., and Behrens, T.E.J. (2019). Human Replay Spontaneously Reorganizes Experience. Cell *178*, 640–652.e14.

Logothetis, N.K., Eschenko, O., Murayama, Y., Augath, M., Steudel, T., Evrard, H.C., Besserve, M., and Oeltermann, A. (2012). Hippocampal-cortical interaction during periods of subcortical silence. Nature *491*, 547–553.

McGinley, M.J., David, S.V., and McCormick, D.A. (2015a). Cortical Membrane Potential Signature of Optimal States for Sensory Signal Detection. Neuron *87*, 179–192.

McGinley, M.J., Vinck, M., Reimer, J., Batista-Brito, R., Zagha, E., Cadwell, C.R., Tolias, A.S., Cardin, J.A., and McCormick, D.A. (2015b). Waking State: Rapid Variations Modulate Neural and Behavioral Responses. Neuron *87*, 1143–1161.

Ngo, H.V., Fell, J., and Staresina, B. (2020). Sleep spindles mediate hippocampal-neocortical coupling during long-duration ripples. eLife *9*, e57011.

Norman, Y., Yeagle, E.M., Khuvis, S., Harel, M., Mehta, A.D., and Malach, R. (2019). Hippocampal sharp-wave ripples linked to visual episodic recollection in humans. Science *365*, eaax1030.

Özkurt, T.E., and Schnitzler, A. (2011). A critical note on the definition of phase-amplitude cross-frequency coupling. J. Neurosci. Methods *201*, 438–443.

R Development Core Team (2010). R: A language and environment for statistical computing (R foundation for Statistical Computing).

Schacter, D.L., Addis, D.R., and Buckner, R.L. (2007). Remembering the past to imagine the future: the prospective brain. Nat. Rev. Neurosci. *8*, 657–661.

Sirota, A., Csicsvari, J., Buhl, D., and Buzsáki, G. (2003). Communication between neocortex and hippocampus during sleep in rodents. Proc. Natl. Acad. Sci. USA *100*, 2065–2069.

Staresina, B.P., Bergmann, T.O., Bonnefond, M., van der Meij, R., Jensen, O., Deuker, L., Elger, C.E., Axmacher, N., and Fell, J. (2015). Hierarchical nesting of slow oscillations, spindles and ripples in the human hippocampus during sleep. Nat. Neurosci. *18*, 1679–1686.

Stigliani, A., Weiner, K.S., and Grill-Spector, K. (2015). Temporal processing capacity in high-level visual cortex is domain specific. J. Neurosci. *35*, 12412–12424.

Tadel, F., Baillet, S., Mosher, J.C., Pantazis, D., and Leahy, R.M. (2011). Brainstorm: a user-friendly application for MEG/EEG analysis. Comput. Intell. Neurosci. *2011*, 879716.

Vaz, A.P., Inati, S.K., Brunel, N., and Zaghloul, K.A. (2019). Coupled ripple oscillations between the medial temporal lobe and neocortex retrieve human memory. Science *363*, 975–978.

STAR★METHODS

KEY RESOURCES TABLE

REAGENT or RESOURCE	SOURCE	IDENTIFIER
Software and algorithms		
AFNI/SUMA	Cox, 1996	https://afni.nimh.nih.gov/Suma
Brainstorm	Tadel et al., 2011	https://neuroimage.usc.edu/brainstorm/
FreeSurfer v5.3	Dale et al., 1999	https://freesurfer.net
iELVIS	Groppe et al., 2017	http://ielvis.pbworks.com/w/page/116347253/FrontPage
Lme4 library	Bates et al., 2014	https://stat.ethz.ch/R-manual/R-devel/library/nlme/html/lme.html
MATLAB (v2017a, v2018b, v2020a)	MathWorks, MA, USA	https://matlab.mathworks.com
Psychtoolbox v3.0.12	Brainard, 1997	http://psychtoolbox.org
R statistical software v4.0.2	R Development Core Team (2010).	https://www.r-project.org
Other		
BlackRock Cerebrus system	BlackRock Microsystems, UT, USA	https://blackrockmicro.com

RESOURCE AVAILABILITY

Lead contact

Further information and requests for resources and reagents should be directed to and will be fulfilled by the Lead Contact, Brett L. Foster (brett.foster@pennmedicine.upenn.edu).

Materials availability

This study did not generate new unique materials.

Data and code availability

The datasets and custom code supporting the current study will be deposited on the National Institute of Mental Health Data Archive (NDA) and released on project completion. Data and code are also available from the lead contact upon reasonable request.

EXPERIMENTAL MODEL AND SUBJECT DETAILS

Human subjects

Intracranial recordings from the human hippocampus were obtained from 18 subjects (S1-18, 8 male, mean age 34.7 years, range 20 – 59 years; see Table S1) undergoing invasive monitor as part of their treatment for refractory epilepsy at Baylor St. Luke's Medical Center (Houston, Texas, USA). Recordings were performed using stereo-electroencephalography (sEEG) depth electrodes (PMT Corp., MN, USA; Ad-Tech Medical Instrument Corp., WI, USA). All experimental protocols were approved by the Institution Review Board at Baylor College of Medicine (IRB protocol number H-18112), with subjects providing verbal and written consent to participate in this study.

METHOD DETAILS

Experimental design

Experimental tasks were all performed at the bedside in a quiet and dimmed patient room (described below). Tasks were presented on an adjustable monitor (1920 × 1080 resolution, 47.5 × 26.7 cm screen size, connected to an iMac running OSX 10.9.4) at a viewing distance of 57 cm. Psychtoolbox functions (v3.0.12) (Brainard, 1997) running in MATLAB (v2017a, MathWorks, MA, USA) were used to program all experiments. Some experimental tasks (Experiment 1 & 4-6) have previously been detailed(Bartoli et al., 2019) and are summarized below.

Experiment 1: Perception task (visual categories)

In the perception task, subjects (S1-17) were presented grayscale images from 10 visual categories (faces, houses, bodies, limbs, cars, words, numbers, instruments, corridors and phase-scrambled noise) in random order (see Figure 2A). Visual stimuli were from a

publicly available corpus, previously used as a visual category localizer in human neuroimaging studies (Stigliani et al., 2015). On each trial, stimuli were shown for 1000 ms, with a random ISI between 1000 - 1500 ms. During the task subjects were required to press a button whenever they detected a specific stimulus being repeated back-to-back (1-back task). Performance was monitored by an experimenter present in the patient room. A total of 15 different stimuli were presented for each category, with 10 random images being repeated (serving as targets), leading to a total of 160 trials. On average the task was 7 minutes in duration.

Experiment 2: Memory task (word-picture paired associates)

In the memory task, subjects (S1-17) performed a paired-associates paradigm with an encoding and retrieval phase. During the encoding phase, subjects were presented with words (e.g., 'coffee', 'nickel') displayed above a box frame containing color photographs of well-known people (e.g., 'Tom Cruise' or 'Julia Roberts'). Word stimuli are selected with limited letter range (4-8), number of syllables (1-3), concreteness rating (600-700) and imaginability rating (600-700) from the Medical Research Council Psycholinguistic Database (https://www.psy.uwa.edu.au/MRCDataBase/uwa_mrc.htm). Word-Picture pairs were presented for 5000 ms, with a self-paced ISI. Subjects pressed a button to advance to the next word-picture pair. A total of 15 word-picture pairs were presented for each task run. After a short delay, the retrieval phase would begin with subjects being presented with only cue words displayed above the box frame, but no picture. Cue words were from a list of 15 old (from encoding phase) and 15 new words. On each trial of the retrieval phase, subjects were required to retrieve the picture associated with the cue. Cue words were presented for 5000 ms and followed by a response period where subjects were asked to provide their memory strength of the cue and associate (see Figure 2). On average the task was 10 minutes in duration.

Experiment 3: Resting task (eyes open / closed)

In the resting task, subjects (S 10,12,16) performed a simple task of alternating eyes open and closed periods, each lasting for 10 s. During the eyes open phase, subjects fixated on a central cross before being prompted to 'close eyes'. During the eyes closed phase, subjects would keep their eyes shut until a brief auditory tone was played to signal the return to eyes open fixation. On average the task was 6 minutes in duration.

Experiments 4-6: Supplemental perception tasks

To further examine our observations of comparable ripple attributes across states, particularly during perceptual tasks, in one subject (S12) we studied three additional perceptual tasks along with examining sleep (below). Details of these tasks have previously been reported (Bartoli et al., 2019) and are briefly summarized here. In the perception-grating task, full screen static grating stimuli were presented for 500 ms at 3 contrast levels (20, 50 & 100%). In the perception-color task, full screen color stimuli (9 colors) were presented for 500 ms. Finally, in the perception-color-object task, color images of different objects (Kiani et al., 2007) were presented for 500 ms.

Experiment 7: Switch task (attention / episodic memory switch tasks)

In the switch task, subjects (S 10,11,15,18) performed two attentional conditions (add and research), two episodic memory conditions (past and future), and rest. During the task, subjects were first presented with a cue indicating the upcoming condition (e.g., 'ADD') for 500 ms. Then the task screen was presented for a maximum of 10 s or until subjects provided a button press to move to the response period. For the rest condition, a fixation cross was presented for 4 s. Finally, following the task screen, there was a response period where subjects were asked to provide a condition specific response. No response period for the rest condition. During the add condition, subjects were asked to find the sum of five single digit numerals (e.g., 3 1 1 2 2) and then respond by choosing the correct sum from 5 alterative choices (e.g., sum? 4, 13, 9, 5, 7). During the search condition, subjects were presented with a matrix of multi-colored letters/numbers and asked to find the one letter/number which was slightly rotated, then respond by choosing the correct color of the target. Prior to testing, subjects were instructed to perform the add and search conditions as quickly and accurately as possible. During the memory conditions (past and future), subjects were presented with statements that either prompted to recall a past event (e.g., 'Think about the last time you ate cake… what flavor was it?', past), or prompt to imagine a future event (e.g., 'Imagine building a snowman', future). Prior to testing, subjects were instructed to visualize past or future events in as much detail as possible. Subjects were required to rate their recall/imaginary experience on a vividness scale of 'strong', 'moderately strong', 'neutral', 'moderately weak', or 'weak'. During the rest task, subjects fixated on a central cross for 4 s (see Figure 6). There were 18 trials per condition, for a total of 90 trials. The task condition presentation sequence was randomized. On average the task was 15 minutes in duration.

Sleep recording

Sleep recordings from subject S12 were also examined to provide an empirical within subject comparison of ripple properties across states. Sleep data was recorded overnight, during which polysomnography (PSG) recordings were performed to allow sleep staging. Following prior methods (Iber and American Academy of Sleep Medicine., 2007; Staresina et al., 2015; Ngo et al., 2020), PSG data was classified into awake, rapid-eye movement (REM) and non-REM (NREM) sleep states. We recorded 736 minutes (12.27 hours) of PSG data where 203 minutes (27.6%) were identified as awake, 78 minutes (10.6%) were identified as REM sleep, and 413 minutes (56.1%) were classified as NREM sleep. The remaining 42 minutes (5.7%) of recording were unable to be classified due to artifacts, and thus excluded from data analysis.

Electrophysiological recording

Intracranial sEEG data was acquired at a sample rate of 2kHz and bandpass of 0.3-500Hz (4th order Butterworth filter) using a BlackRock Cerebus system (BlackRock Microsystems, UT, USA). Initial recordings were referenced to a selected depth electrode contact within the white matter, distant from gray matter or pathological zones. During recordings, stimulus presentation was tracked using a photodiode sensor (attached to stimulus monitor) synchronously recorded at 30kHz. All additional data processing was performed offline.

Electrode localization and selection

To identify electrodes located within the hippocampal formation, a post-operative CT scan was co-registered to a pre-operative T1 anatomical MRI scan for each subject, using FSL and AFNI (Cox, 1996; Dale et al., 1999). The volume location of each electrode was identified by clear hyperintensities on the aligned CT using AFNI and visualized using iELVis software functions in MATLAB (v2016a, MathWorks, MA, USA) (Groppe et al., 2017). Within subjects, electrodes located within or at the margin of the hippocampal formation were identified, along with electrodes located within the white matter for each depth electrode targeting the medial temporal lobe. As detailed below, white matter electrodes were employed to re-reference hippocampal sites within each probe. Each participant performed several experimental tasks during sEEG recordings.

QUANTIFICATION AND STATISTICAL ANALYSIS

Preprocessing and spectral decomposition

All signal processing was performed using custom scripts in MATLAB (v2018b, MathWorks, MA, USA). First, raw EEG signals were inspected for line noise, recording artifacts or interictal epileptic spikes. Electrodes with clear epileptic or artifactual activity were excluded from further analysis. Second, we identified sEEG probes targeting the medial temporal lobe, identifying which probes had electrode contacts within or at the boundary of the hippocampus. For each identified probe, hippocampal electrode contacts were notch filtered (60 Hz and harmonics) and re-referenced to a proximal electrode contact within the white matter on the same probe. Finally, Re-referenced signals from each hippocampal electrode were down sampled to 1kHz and spectrally decomposed using Morlet wavelets, with center frequencies spaced linearly from 2 to 200 Hz in 1 Hz steps (7 cycles).

Ripple detection and rejection

After pre-processing steps, ripple events were identified in three general stages: i) time domain detection for identifying putative ripple events; ii) frequency domain assessment for accepting/rejecting ripple events; iii) electrode wise ripple count thresholding for inclusion/exclusion. Analytic criteria were based on prior human hippocampal ripples studies (Staresina et al., 2015; Helfrich et al., 2019; Jiang et al., 2019, 2020; Ngo et al., 2020), as detailed below.

Signals from identified hippocampal electrodes (i.e., continuous voltage time-series filtered and re-referenced) were first band-pass filtered from 80 to 120 Hz (ripple band) using a 4th order FIR filter. This ripple band range was selected based on prior studies in the human hippocampus (Bragin et al., 1999; Axmacher et al., 2008; Helfrich et al., 2019; Jiang et al., 2019; Norman et al., 2019; Vaz et al., 2019; Ngo et al., 2020), which report ripple range activity at lower frequencies than observed in the rodent (Buzsáki, 2015). Next, the root mean square (RMS) of the band-passed signal was calculated and smoothed using a 20-ms window. Ripples were detected based on amplitude and duration thresholds of this RMS time course. Whereby, ripple events were identified as having an RMS amplitude above 2.5, but no greater than 9, standard deviations from the mean. Ripple duration was defined as the supra-threshold time of the RMS-signal. Detected ripple events with a duration shorter than 38 ms (corresponding to 3 cycles at 80 Hz) or longer than 500 ms, were rejected. In addition to the amplitude and duration criteria the spectral features of each detected ripple event were examined. To do so, spectrally decomposed data (i.e., continuous time-series notch filtered, re-referenced and decomposed using Morlet wavelets), was used to calculate the frequency spectrum for each detected ripple event by averaging the normalized instantaneous amplitude between the onset and offset of the ripple event for the frequency range of 2-200 Hz. Spectral amplitude was normalized to a percent change signal by applying a baseline correction at each frequency based on the mean amplitude of the entire recording for a given electrode and frequency. For each detected ripple frequency spectrum, we examined the number and properties of spectral peaks. Spectral peaks were identified using the *findpeaks.m* MATLAB function. For every peak detected, the height, prominence, peak frequency and peak width were employed for our rejection evaluation. The impetus for these steps was to ensure that detected ripple events reflected high-frequency narrowband bursts limited to the ripple band range, rather than more broadband spectral changes increasing amplitude within and beyond the ripple band range (see Figure 1), driven by recording of ictal transient events in the time domain voltage. To do so we applied three criteria: First, ripple-events with a maximal spectral amplitude increase greater than 600% from the baseline were rejected. Second, genuine ripple events should display a unitary and predominant spectral peak with the ripple band range. Therefore, if no single prominent peak (ripple-peak) within the ripple band was identified, the event was rejected. Lastly, genuine ripple events should display a limited narrowband burst; therefore, if the ripple-peak had a wide peak width (more broadband spectral change) or a prominent high frequency activity (large peaks in 120 – 200 Hz), the event was rejected.

To quantify these criteria, we implemented the following steps for rejection 1) events with more than one peak in the ripple band; 2) events where the most prominent and highest peak was outside the ripple band and sharp wave band for a frequencies > 30 Hz (as peaks found below 30 Hz may reflect the sharp wave that usually accompanies ripple events; Jiang et al., 2020); 3) events where

ripple-peak width was greater than 3 standard deviations from the mean ripple-peak width calculated for a given electrode and recording session; and 4) events where high frequency activity peaks exceed 80% of the ripple peak height. After applying the trial-wise spectral rejection, we calculated the number of ripples detected and ripple rejection rate for each electrode. We then rejected any electrode with a low ripple count (< 20 ripples detected per electrode per task) or high rejection rate (greater than 30% rejection rate), as these likely reflect weak or noisy recordings.

For identified ripples, there were four main attributes we examined: 1) ripple rate (Hz) calculated by using the number of detected ripple events divided by recording time in seconds, 2) ripple duration (ms), 3) ripple max amplitude (μV) calculated using ripple band-passed signal, and 4) ripple peak frequency (Hz).

Surrogate data analysis

Figure 1 provides an example of our ripple detection approach. To further benchmark this methodology, surrogate data were generated as a signal control. After pre-processing steps (i.e., continuous voltage time-series filtered and re-reference), signals from an identified sample electrode were used as the 'template' to generate a surrogate signal via iterative Amplitude Adjusted Fourier Transform (iAAFT) algorithm (Lancaster et al., 2018). The goal of the surrogate signal is to preserve key statistical features of the original signal while disrupting local temporal events like ripple. Each iteration randomly shuffles the data points from the 'template' while adjusting its frequency spectrum and amplitude to match the original. The final surrogate data preserves the overall spectrum profile and amplitude of the template and destroys certain temporal features of the original data. The final surrogate data were then passed through the same ripple detection and rejection method outlined above. For the ripples identified from the surrogate data, we examined the four main attributes (ripple rate, ripple duration, ripple max amplitude and ripple peak frequency) and compared them with ripples identified from the sample data (See Figures 1 and S1).

Phase-amplitude coupling analysis

To assess the coupling of hippocampal ripples to other well know electrographic sleep signals (e.g., spindles and slow oscillations) during NREM sleep, we performed phase-amplitude coupling analysis. First, NREM sleep recordings from subject S12 were pre-processed as detailed above (notch filtered and re-referenced). Next, we quantified a comodulogram coupling matrix defined by phase frequencies between 2-9 Hz and amplitude frequencies between 10 – 170 Hz (all with 1 Hz steps). A direct phase-amplitude coupling (PAC) value was calculated for each phase-amplitude pair using the *bst_pac* function of BrainStorm3 (Tadel et al.,2011). The direct PAC metric is a pairwise modulation index score (a.u.) ranging from 0 to 1, where higher values indicate stronger temporal coupling between phase and amplitude frequency pairs (Canolty et al., 2006 and Özkurt and Schnitzler 2011).

Statistical analysis

Ripple event data was subject to quantification using parametric and non-parametric statistical methods as appropriate for underlying data distributions. Mixed-effects models, using subject and electrode as random effects, were employed to account for the nesting of multiple electrodes within each subject. Statistical analyses were carried out using R statistical software (R Development Core Team, 2010). For specific statistical test information and outcomes see Results.

Cell Reports, Volume *35*

Supplemental information

Stability of ripple events during task engagement in human hippocampus

Yvonne Y. Chen, Lyndsey Aponik-Gremillion, Eleonora Bartoli, Daniel Yoshor, Sameer A. Sheth, and Brett L. Foster

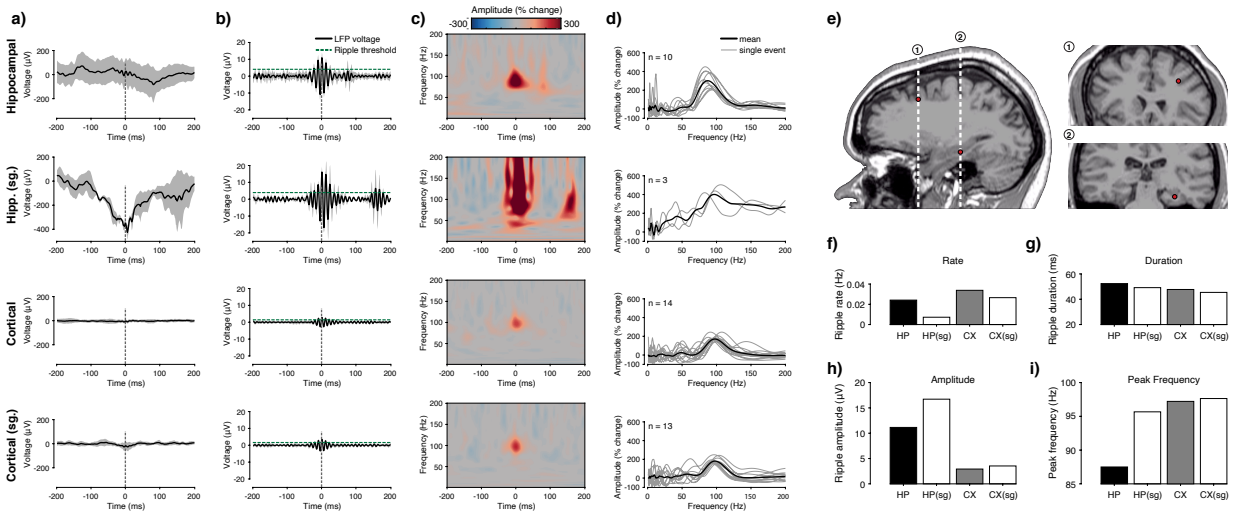

Figure S1. Ripple detection in hippocampus and cortex for real and surrogate data. Related to Figure 1. a) Example raw voltage traces from hippocampus and cortex showing mean ripple triggered trace after artifact rejection for real and surrogate data (same data as Figure 1; subject S10). Here and below, time zero aligns to the maximal ripple amplitude, and error shading reflects s.d. **b)** Ripple-band (80–120 Hz) voltage traces for example hippocampal, hippocampal surrogate, cortical and cortical surrogate recording (same data as (a)). Green dashed line reflects the ripple detection threshold for this electrode. **c)** Spectrograms are shown for the example hippocampal, hippocampal surrogate, cortical and cortical surrogate ripple events, color maps reflect percentage change in amplitude relative to the total signal mean. Ripple events detected in the hippocampus (n = 10) display a high-frequency narrow band time-frequency representation, while the few hippocampal surrogate ripple events (n = 3) display a much more broadband frequency representation due to the voltage deflection shown in (a). Cortical recording and its surrogate ripple events display a restricted and reduced narrow band time-frequency representation likely due to small amplitude change shown in (a & b). **d)** Normalized amplitude spectra (percentage change) for the hippocampal, hippocampal surrogate, cortical and cortical surrogate averaged over the detected ripple event onset/offset window. While the hippocampal ripple events display a predominant spectral peak in the ripple-band range, the hippocampal surrogate ripple events show multiple spectral peaks outside of the ripple-band. Cortical and its surrogate ripple events show a highly similar single peak in the ripple-band range, whose amplitude change is less pronounced. **e)** Anatomical location of example hippocampal and cortical electrodes in subject S10. Sagittal view (left) shows longitudinal position of each probe, with the white dashed lines indicating the respective coronal slices (right; ①cortical & ②hippocampal). **f-i)** Ripple attributes are shown for example hippocampal (HP), hippocampal surrogate (HP(sg)), cortical (CX) and cortical surrogate (CX(sg) ripple events: rate (f); duration (g), amplitude (h) and peak frequency (i).

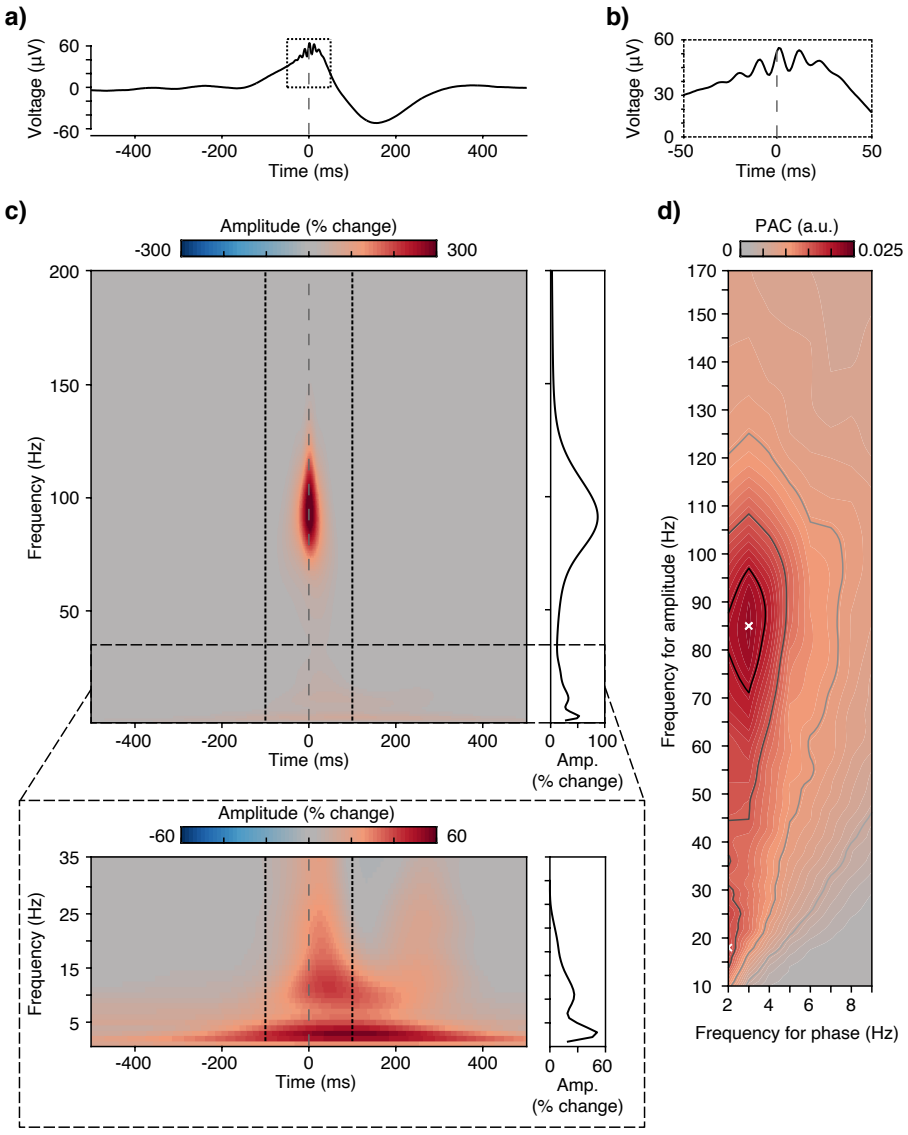

Figure S2. Ripples during NREM sleep. Related to Figure 5. a) Subject (S12) averaged ripple-triggered raw voltage trace for NREM sleep, here and below, time zero aligns to the maximal ripple amplitude. This raw voltage trace highlights the nesting of ripples in the slow oscillation. **b)** Zoom in average ripple-trigged raw voltage for NREM sleep. **c)** Subject averaged NREM sleep ripple-triggered spectrograms for 1-200 Hz frequency range (top left) and zoom in 1-35 Hz frequency range (bottom left), color maps reflect percentage change in amplitude relative to the total signal mean. Subject averaged normalized amplitude spectra (percent change) for 1-200 Hz frequency (top right) and zoom in 1-35 Hz frequency range (bottom right), estimated over -/+ 100 ms window denoted by the black dashed line on the spectrograms. Hippocampal ripples displayed a narrow band time-frequency (80-120 Hz) representation during NREM sleep. Importantly, there is ripple time-locked amplitude increases at the spindle-frequency (10 - 15 Hz) and slow oscillation frequency (<4 Hz), suggesting nesting of ripples during spindle and slow oscillations. **d)** Phase-amplitude coupling (PAC) comodulogram matrix between low (2 – 9 Hz; phase) and high (10 – 170 Hz; amplitude) frequency ranges during NREM sleep. White x markers indicate the top two local maxima PAC values, indicating clear coupling between ripple band (max 85 Hz) and spindle band (max 18 Hz) amplitude with slow wave frequency phase (2-4 Hz). Note: high-pass filters during data recording limited examination of the full slow oscillation range (<1 Hz).

Sub	Sex	Age	Task Performed	Elecs. in Hipp.			Included elecs.		
				Tot.	*L*	*R*	*Tot.*	*L*	*R*
1	F	37	P, M	8	5	3	2	0	2
2	F	32	P, M	3	3	-	3	3	-
3	F	59	P, M	9	9	-	4	4	-
4	M	53	P, M	10	6	4	3	3	0
5	F	32	P, M	1	1	-	1	1	-
6	M	25	P, M	13	9	4	13	9	4
7	M	26	P, M	3	3	-	1	1	-
8	F	33	P, M	7	4	3	4	4	0
9	F	27	P, M	14	7	7	10	6	4
10	F	39	P, M, R, S	12	5	7	10	3	7
11	F	40	P, M, S	7	3	4	4	0	4
12	F	33	P, M, R, additional P tasks, sleep	6	-	6	6	-	6
13	M	22	P, M	5	5	-	4	4	-
14	M	39	P, M	4	3	1	4	3	1
15	M	30	P, M, S	5	-	5	5	-	5
16	F	20	P, M, R	12	12	-	6	6	-
17	M	43	P, M	8	3	5	2	1	1
18	M	34	S	12	7	5	12	7	5
				139	85	54	94	55	39

Table S1. Subject and electrode information. Related to STAR Methods: *Experimental Model and Subject Details*. For each subject (1-18) demographic and experimental information is reported in the following order: Sex (Male/Female); Age at time of experiment (years); Experimental tasks performed: Perception (P), Memory (M), Resting (R), Switch (S), other additional Perception tasks and sleep recording; Identified electrode count within hippocampus and hemisphere (Left/Right); Included electrode count within hippocampus and hemisphere (Left/Right).

Tasks	**Ripple attributes**			
NREM –	*Rate*	*Duration*	*Amplitude*	*Frequency*
Perception	t(43.8) = 5.592, p < 0.0001	t(43.9) = 1.578, p = 0.8110	t(44) = 3.472, p = 0.0291	t(43.8) = -5.817, p < 0.0001
Memory	t(43.8) = 6.380, p < 0.0001	t(43.8) = 3.956, p = 0.0077	t(44) = 6.044, p < 0.0001	t(43.8) = -5.832, p < 0.0001
Resting	t(43.8) = 5.098, p = 0.0002	t(43.9) = -0.272, p = 1.000	t(44) = 4.248, p = 0.0032	t(43.8) = -5.908, p < 0.0001
P-grating	t(44.1) = 5.129, p = 0.0002	t(44) = 2.878, p = 0.1224	t(44) = 3.996, p = 0.0068	t(44.1) = -2.775, p = 0.1588
P-color	t(43.8) = 6.260, p<0.0001	t(43.9) = 2.514, p = 0.2533	t(44) = 6.442, p < 0.0001	t(43.8) = -6.105, p < 0.0001
P-color obj	t(44.7) = 4.802, p = 0.0006	t(44.4) = 2.735, p = 0.1650	t(44.1) = 3.654, p = 0.0179	t(44.6) = -4.802, p = 0.0057
Awake	t(43.8) = 6.366, p < 0.0001	t(43.9) = 3.672, p = 0.0170	t(44) = 2.835, p = 0.1341	t(43.8) = -7.010, p < 0.0001
REM	t(43.8) = 7.283, p < 0.0001	t(43.9) = 4.917, p = 0.0004	t(44) = 4.921, p = 0.0004	t(43.8) = -7.854, p < 0.0001

Table S2. Comparing ripple attributes between NREM sleep and cognitive tasks and sleep stages. Related to Figure 5. Pairwise Tukey's range test comparing ripple attributes: rate, duration, amplitude and peak frequency between NREM sleep and cognitive tasks and other sleep stages, p-value is adjusted for comparing a family of 9 estimates.

	Ripple Rate	
Conditions	*Past -*	*Future -*
Add	t(161) = 6.220, p < 0.0001	t(161) = 5.069, p < 0.0001
Search	t(161) = 6.169, p < 0.0001	t(161) = 5.018, p < 0.0001
Rest	t(161) = 5.918, p < 0.0001	t(161) = 4.767, p < 0.0001

Table S3. Comparing ripple rates between episodic memory conditions and other attentional and rest conditions. Related to Figure 7. Pairwise Tukey's range test comparing ripple rate between episodic conditions (Past and Future) and other conditions, p-value is adjusted for comparing a family of 5 estimates.